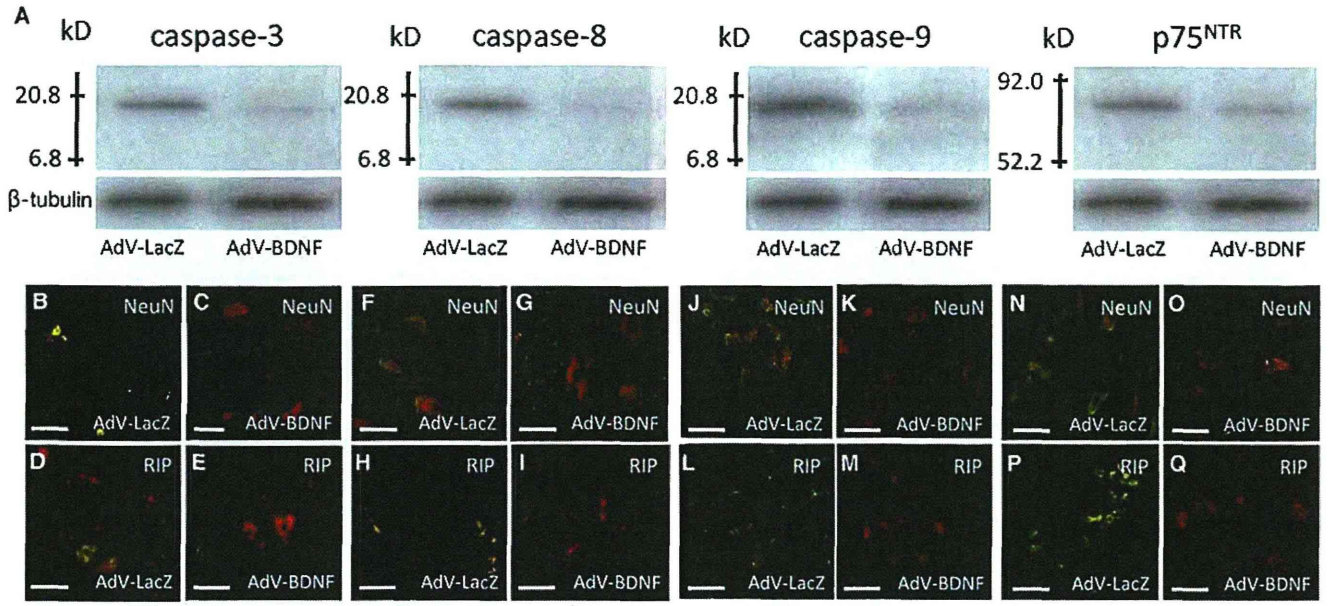

Figure 5. Immunoblot analysis showing expression of activated-caspase-3, caspase-8, caspase-9, and p75^{NTR} (**A**) and photomicrographs of double-staining immunofluorescence (**B–Q**). The active form of each of these caspases was downregulated in the *AdV-BDNF* gene–transfected *twy/twy* mice (**A:** upper right on each panel) compared with the *AdV-LacZ* gene–transfected *twy/twy* mice (**A:** upper left on each panel). Photomicrographs show double-stained immunofluorescence in the gray matter and the white matter of the *twy/twy* mouse at the maximal compression site for activated-caspase-3/NeuN (**B** and **C**), /RIP (**D** and **E**), caspase-8/NeuN (**F** and **G**), /RIP (**H** and **I**), caspase-9/NeuN (**J** and **K**), /RIP (**L** and **M**) p75^{NTR}/NeuN (**N** and **O**), and /RIP (**P** and **Q**) at 4 weeks after *AdV-LacZ* and *AdV-BDNF* gene transfection. Decreased immunopositivity for activated-caspase-3, caspase-8, caspase-9, and p75^{NTR} were noted in neurons and oligodendrocytes of the *AdV-BDNF* gene–transfected *twy/twy* mice compared with the *AdV-LacZ* gene–transfected *twy/twy* mice. Scale bar = 10 μm (**B–Q**). NeuN indicates neurons; RIP, reactive immunology protein.

2. Such targeted delivery of *AdV-BDNF* to the compressed area of the spinal cord resulted in downregulation of the caspase-3 pathway apoptotic cascade and a significant decrease in the number of apoptotic cells present.
3. BDNF gene delivery also resulted in a significant promotion of NF and NG2 immunopositivity in the compressed spinal cord, which is indicative of decreased neuronal loss and demyelination.

These encouraging findings should be discussed in terms of neuroprotective effects and technical advantages.

In a series of previous studies using acute injury models, our group evaluated the feasibility and efficacy of retrograde gene delivery, using recombinant adenovirus vectors[29] through the mouse sternomastoid muscle, innervated by the spinal accessory nerve, into the injured cervical spinal cord.[18,19,30] In these studies, the expression of the β-galactosidase (*AdV-LacZ*) marker gene was found in the cervical spinal cord from 4 to 6 weeks after the injection of adenovirus vector, and transduction efficacy was confirmed in 87.5% to 98.9% of the surviving cervical spinal cord motor neurons within 3 days after the injection.[18,19] In this study, we found abundant β-galactosidase-labeled cells in the *twy/twy* mouse spinal cord 4 weeks after injection of *AdV-LacZ* gene into the sternomastoid muscle bilaterally, in cells which were also immunoreactive to various neural cell markers, including motor neurons and glial cells. Hence, these were similar results in terms of successful retrograde gene delivery into a chronic spinal cord lesion to those obtained with acute spinal cord injury.[31–33] It should be noted that the efficiency of retrograde delivery of neuropeptide genes is influenced by various factors,[34] such as the local secretion of proteins from AdV-infected muscles, uptake and retrograde axonal transport of AdV in motor neurons, and secretion of proteins in AdV-infected muscles into the systemic circulation. In this context, our previous study suggested that *AdV-LacZ* is transported *via* retrograde axonoplasmic flow through axons but not through the systemic circulation because no gene expression was noted in other body organs.[35] The present results indicate that retrograde gene delivery *via* intramuscular injection into the chronically compressed spinal cord was attained not only to the spinal motor neurons and interneurons, but also to proglial cells that may have been induced by acute and/or chronic mechanical compression.

Several investigators have reported that exogenous administration of BDNF promotes neural cell survival, alleviates neuronal atrophy,[36] facilitates axonal regeneration,[37] prevents apoptosis,[38,39] enhances differentiation of neuronal stem cells to neurons, improves motor function,[40] and induces glial cell proliferation as well as axonal outgrowth and myelination.[41] Apoptosis and necrosis after traumatic cord injury occur through different pathways in the neuronal tissue. Apoptosis of neurons and oligodendrocytes involves the activation of caspase-3 after acute spinal cord injury.[42] In our previous study in *twy/twy* mouse using the TUNEL method to identify apoptotic cells,[27] no TUNEL-positive cells were observed

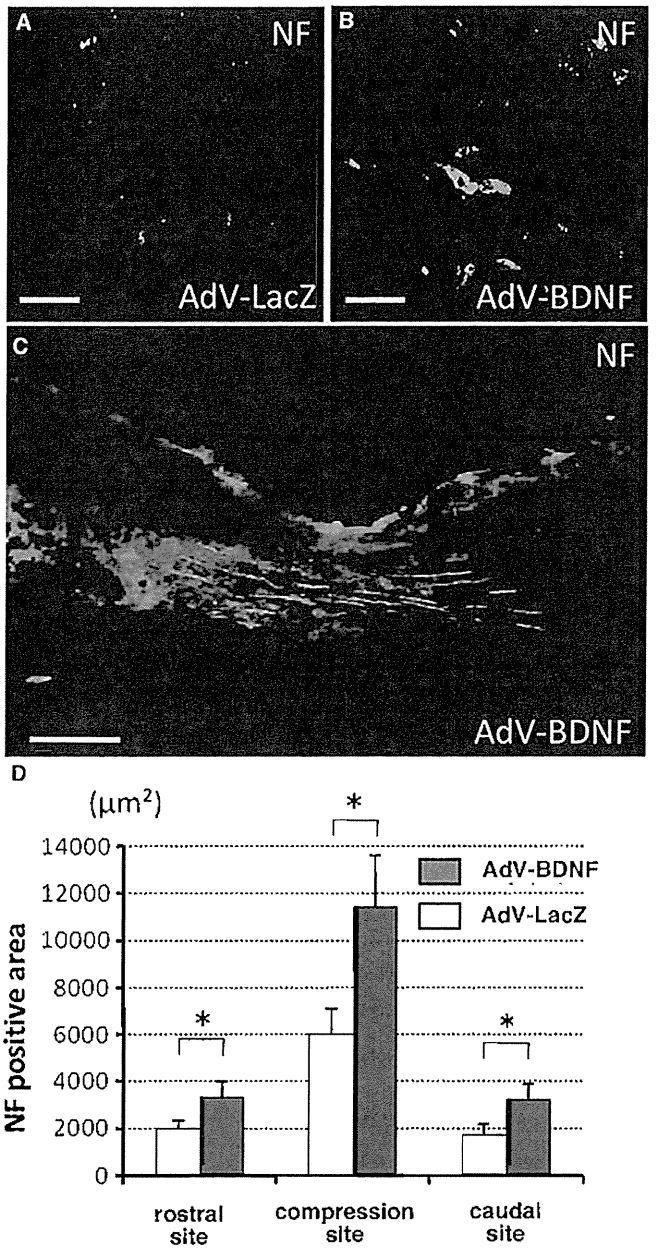

Figure 6. Photomicrographs showing immunopositivity for NF (A–C) in *twy/twy* mice transaxial (A and B) and sagittal (C) sections of the spinal cord at 4 weeks after *AdV-LacZ* or *AdV-BDNF* gene transfection. In *twy/twy* mice transfected with the *AdV-BDNF* gene, the levels of NF immunopositivity in neurons of the gray matter were increased (B and C) compared with that seen in the mice transfected with the *AdV-LacZ* gene (A). The NF-immunopositive areas were significantly greater at all anatomical sites measured in the *AdV-BDNF* gene–transfected mice (n = 3) than that in the *AdV-Lac Z* gene–transfected mice (n = 3) (D). Data are mean ± SD. **P* < 0.01. Scale bar = 500 μm (C), 10 μm (A and B). NF indicates neurofilament.

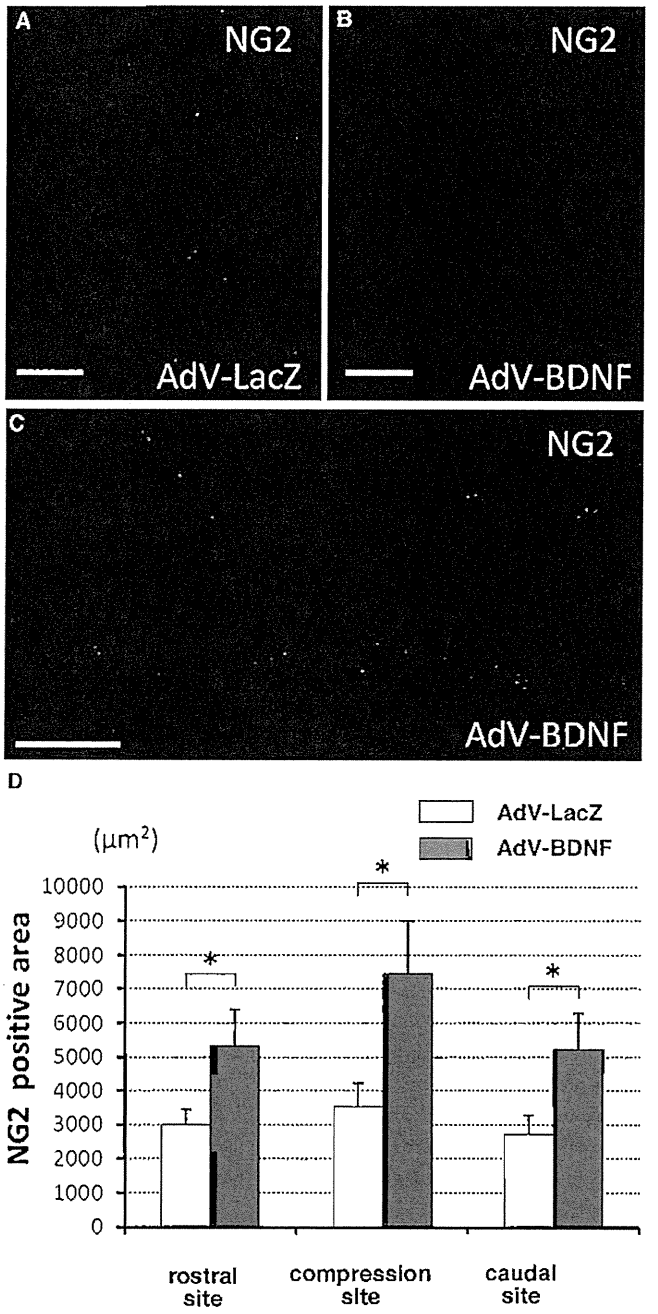

Figure 7. Photomicrographs showing NG2-immunopositivity in *twy/twy* mice transaxial (A and B) and sagittal (C) sections of the spinal cord at 4 weeks after *AdV-LacZ* (A) or *AdV-BDNF* (B and C) gene transfection. NG2-immunopositivity in glial cells was increased after *AdV-BDNF* gene transfection (B and C) compared with *AdV-LacZ* gene transfection (A). The NG2-immunopositive areas in the *AdV-BDNF* gene–transfected mice (n = 3) were significantly greater at all anatomical sites measured than that in *AdV-LacZ* gene–transfected mice (n = 3) (D). Data are mean ± SD. **P* < 0.01. Scale bar = 500 μm (C), 10 μm (A and B).

in 16-week-old *twy/twy* mice, whereas both TUNEL-positive and caspase 3-positive cells were detected in the gray and white matters of the spinal cord of 24-week-old mice. Our previous data indicated that transgene expression of the targeted AdV persists for 4 to 6 weeks after injection,[18] and thus in this study, we attempted to perform intramuscular *AdV-BDNF* injection in 18-week-old *twy/twy* mice with relatively mild cord compression and observed the subjects

until they became 22-week-old, showing an increased spinal cord compression, although no image analysis (radiography or computed tomography) was performed before the histological study. We found attenuation of apoptosis of neurons and oligodendrocytes at 4 weeks after injection. Our current observations further suggest that this reduction in apoptosis was attributable to downregulation of the caspase-3, -8, and -9 mediated pathway in the *twy/twy* mouse spinal cord. Most interestingly in oligodendrocytes, $p75^{NTR}$ not only serves as a low affinity receptor from neurotrophins, but it also mediates the effects of myelin inhibitors.[43] Recently, enhanced neurological recovery was identified in $p75^{NTR}$ knockout mice,[44] a process integral to neuronal survival and intracellular reparative mechanisms after compressive spinal cord injury.[45] Hence, the downregulation of $p75^{NTR}$ after *AdV-BDNF* injection that we have observed may indicate suppression of apoptosis, particularly of oligodendrocytes in mechanically compressed spinal cord.

The present results also showed that retrograde *AdV-BDNF* gene administration into the sternomastoids preserved or even increased levels or even NF and NG2 in the neurons and oligodendrocyte precursors in the chronically compressed spinal cord. NF is an essential cytoskeletal element of axonal processes and hence its enhanced levels after BDNF transfection may function in enhancing regional axonal tegeneration and functional recovery,[24] although it was impossible to estimate locomotor function because of aging-related hyperostotic ankylosing leg joints in the *twy/twy* mice.[21] The presence of oligodendrocytes that survive even under demyelinating insults to the spinal cord does not correlate to remyelination.[46] Instead, endogenous oligodendrocyte progenitor cells labeled by NG2 indicate proliferation of cycling cells,[47] and they are expected to contribute to myelin repair.[48,49] After spinal cord injury, expression and localization of NG2 were identified in the residual white matter,[33] and we also observed NG2-positive neuronal cells in the compressed as well as less compressed (rostral and caudal sites) cord segments of the *twy/twy* mice. Although the question as to whether BDNF reduces oligodendrocyte apoptosis or not remains unsolved, the cell is expected to produce the full-length form of trkB, and its survival may depend on MAPK signaling pathway downstream of TrkB.[50] BDNF is reported to induce proliferation of oligodendrocytes and myelination of regenerating axons after spinal cord injury.[51] Hence, the present finding of increased NG2 immunoreactivity after *AdV-BDNF* gene transfection could be a further indication that BDNF exerts antiapoptotic effects on neural cells including oligodendrocytes.

Finally, there were several limitations to the translational interpretation of these experiments. These included (1) side effects of the viral infection on the general and the local muscle after injection; (2) a possibility of transfection to the dorsal neuron ganglion and the gray matter of the dorsal horn by retrograde gene delivery and the side effects thereof; (3) the issue of muscle injection selection sites suitable for the injured site; (4) the impossibility to perform neurological assessments to evaluate the effects of suppression of apoptosis in spinal neurons and oligodendrocytes, based on the response to external stimuli or testing motor skills through behavior scores—the animal model joints present general ankylosis followed by muscle atrophy and fibrosis. Further studies are required to clarify these points. Nonetheless, if these issues are resolved, then the targeted retrograde *AdV-BDNF* gene delivery method that has been detailed in this study could be a potentially useful therapeutic intervention to promote neuronal and oligodendrocyte survival in those who suffer from a compressed spinal cord.

➢ Key Points

- ❑ Retrograde delivery of the control *LacZ* marker gene *via* injection into the bilateral sternomastoid muscles successfully transfected neurons and glial cells, including oligodendrocytes, in the *twy/twy* mouse spinal cord with spontaneous chronic mechanical compression.
- ❑ Retrograde delivery of the *AdV-BDNF* gene resulted in a significant neuroprotective effects in the compressed spinal cord, indicated by a decrease in the number of TUNEL-positive apoptotic cells, downregulation of the caspase apoptotic pathway, and the increased presence of NF- and NG2-immunoreactive neural cells compared with controls.
- ❑ Targeted retrograde *AdV-BDNF* gene delivery is considered a potentially useful therapeutic tool for neuronal and oligodendrocyte survival in chronic spinal cord compression.

Acknowledgments

This work was supported in part by Grant-in-Aid to HB, HN, and KU for General Scientific Research of the Ministry of Education, Science and Culture of Japan (grant numbers B-12470305, C-13671499, C-15591571, B-16390435, B-18390411, and B-19791023). This work was also supported in part by grants to HB from the Investigation Committee on Ossification of the Spinal ligaments, Public Health Bureau of the Japanese Ministry of Labor, Health and Welfare (2005–2009). An International Postgraduate Scholarship (2009–2012) was awarded to ARD from the Ministry of Education, Science and Culture of Japanese Government.

References

1. Katoh K, Ikata T, Katoh S, et al. Induction and its spread of apoptosis in rat spinal cord after mechanical trauma. *Neurosci Lett* 1996; 216:9–12.
2. Li GL, Brodin G, Farooque M. Apoptosis and expression of bcl-2 after compression trauma to rat spinal cord. *J Neuropathol Exp Neurol* 1996;55:280–9.
3. Crowe MJ, Bresnahan JC, Shuman SL, et al. Apoptosis and delayed degeneration after spinal cord injury in rats and monkeys. *Nat Med* 1997;3:73–6.
4. Shuman SL, Bresnahan JC, Beattie MS. Apoptosis of microglia and oligodendrocytes after spinal cord contusion in rats. *J Neurosci Res* 1997;50:798–808.

ahara S, Yone K, Sakou T, et al. Induction of apoptosis signal lating kinase 1 (ASK1) after spinal cord injury in rats: possible lvement of ASK1-JNK and p38 pathways in neuronal apopto- *Neuropathol Exp Neurol* 1999;58:442–50.
Y, Yamamoto T, Sugiyama Y, et al. Apoptotic cells associated Wallerian degeneration after experimental spinal cord injury: ssible mechanism of oligodendroglial death. *J Neurotrauma*);16:946–52.
iL, Farooque M, Holtz A, et al. Apoptosis of oligodendro- : occurs for long distances away from the primary injury after pression trauma to rat spinal cord. *Acta Neuropathol* 1999;98: -80.
XZ, Xu XM, Hu R, et al. Neural and glial apoptosis after matic spinal cord injury. *J Neurosci* 1997;17:5395–406.
SK, Wilford GG, Matzelle DC, et al. Calpain and methylpred- lone inhibit apoptosis in rat spinal cord injury. *Ann N Y Acad* 999;860:261–9.
a S, Yone K, Ichidou Y, et al. Apoptosis following spinal injury in rats and preventive effect of *N*-methyl-D-aspartate otor antagonist. *J Neurosurg* 1999;91:98–104.
enberg MJ, Eggers R, Boer GJ, et al. Adeno-associated vectors as agents for gene delivery: application in disorders trauma of the central nervous system. *Methods* 2002;28: -94.
driks WT, Ruitenberg MJ, Blits B, et al. Viral vector-mediated : transfer of neurotrophins to promote regeneration of the ed spinal cord. *Prog Brain Res* 2004;146:451–76.
un J, Puzis R, Pearse D, Gage FH, Bunge MB. Muscle injection AV-NT3 promotes anatomical reorganization of CST axons improves behavioral outcome following SCI. *J Neurotrauma* 9;26:941–53.
mes AJ, Caudle RM, O'Connell BC, Iadarola MJ. Adenoviral : transfer to spinal-cord neurons: intratheeal vs. intraparenchy- administration. *Brain Res* 1998;793:1–6.
mgartner BJ, Shine HD. Neuroprotection of the spinal moto- ons following targeted transduction with an adenoviral vector ying gene for glial cell line-derived neurotrophic factor. *Exp rol* 1998;153:102–12.
abe K, Ohashi T, Sakamoto T, et al. Rescue of lesioned adult pinal motoneurons by adenoviral gene transfer of glial cell line- ved neurotrophic factor. *J Neurosci Res* 2000;60:511–9.
umoto T, Kawazoe Y, Shen JS, et al. Adenoviral gene transfer DNF, BDNF, and TGF beta 2, but not CNTF, cardiotrophin-1 GF1, protects injured adult motoneurons after facial nerve sion. *J Neurosci Res* 2003;72:54–64.
ajima H, Uchida K, Kobayashi S, et al. Targered retrograde : delivery into the injured cervical spinal cord using recombi- : adenovirus veetor. *Neurosci Lett* 2005;385:30–5.
ajima H, Uchida K, Kobayashi S, et al. Rescue of rat anterior n neurons after spinal cord injury by retrograde transfection of novirus vector carrying brain-derived neurotrophic factor gene. *urotrauma* 2007;24:703–12.
ieyama T, Hashizume Y, Ando T, et al. Spinal cord morphology pathology in ossification of the posterior longitudinal ligament. *n* 1995;118:263–78.
a H, Maezawa Y, Imura S, et al. Quantitative analysis of the spi- cord motoneuron under chronic compression: an experimental rvation in the mouse. *J Neurol* 1996;243:109–16.
a H, Maezawa Y, Uchida K, et al. Three-dimensional topo- hic analysis of spinal accessory motoneurons under chronic hanical compression: an experimental study in the mouse. *urol* 1997;244:222–9.
ida K, Baba H, Maezawa Y, et al. Histological investigation pinal cord lesions in the spinal hyperostotic mouse (*twy/twy*): phological changes in anterior horn cells and immunoreactivity eurotrophic factors. *J Neurol* 1998;245:781–93.
ida K, Baba H, Maezawa Y, et al. Progressive changes in ofilament proteins and growth-associated protein-43 immuno- rivities at the site of cervical spinal cord compression in *twy/twy* . *Spine* 2002;27:480–6.
25. Uchida K, Baba H, Maezawa Y, et al. Increased expression of neurotrophins and their receptors in the mechanically compressed spinal cord of the spinal hyperostotic mouse (*twy/twy*). *Acta Neuropathol* 2003;106:29–36.
26. Okawa A, Nakamura I, Goto S, et al. Mutation in Npps in a mouse model of ossification of the posterior longitudinal ligament of the spine. *Nat Genet* 1998;19:271–3.
27. Yamaura I, Yone K, Nakahara S, et al. Mechanism of destructive pathologie change in the spinal cord under chronic mechanical compression. *Spine* 2002;27:21–6.
28. Takenouchi T, Setoguchi T, Yone K, et al. Expression of apoptosis signal-regulating kinase 1 in monse spinal cord under chronic mechanical compression: possible involvement of the stress-activated mitogen-activated protein kinase pathways in spinal cord cell apoptosis. *Spine* 2008;33:1943–50.
29. Miyake S, Makimura M, Kanegae Y, et al. Efficient generation of recombinant adenoviruses using adenovirus DNA-terminal protein complex and a cosmid bearing the full-length virus genome. *Proc Natl Acad Sci U S A* 1996;93:1320–24.
30. Kitamura S, Sakai A. A study on the localization of the sternocleidomastoid and trapezius motoneurons in the rat by means of the HRP method. *Anat Rec* 1982;202:527–36.
31. Horner PJ, Power AE, Kempermann G, et al. Proliferation and differentiation of progenitor cells throughout the intact adult rat spinal cord. *J Neurosci* 2000;20:2218–28.
32. Ishii K, Toda M, Nakai Y, et al. Increase of oligodendrocyte progenitor cells after spinal cord injury. *J Neurosci Res* 2001;65:500–7.
33. Zai LJ, Wrathall JR. Cell proliferation and replacement following contusive spinal cord injury. *Glia* 2005;50:247–57.
34. Haase G, Pettmann B, Vigne E, et al. Adenovirus-mediated transfer of the neurotrophin-3 gene into skeletal muscle of *pmn* mice: therapeutic effects and mechanisms of action. *J Neurol Sci* 1998;160:S97–105.
35. Nakajima H, Uchida K, Kobayashi S, et al. Target muscles for retrograde gene delivery to specifie spinal cord segments. *Neurosci Lett* 2008;435:1–6.
36. Novikova LN, Novikov LN, Kellerth JO. Survival effects of BDNF and NT-3 on axonotomized rubrospinal neurons depend on the temporal pattern of neurotrophin administration. *Eur J Neurosci* 2000;12:776–80.
37. Kishino A, Ishige Y, Tatsuno T, et al. BDNF prevents and reverses adult rat motor neuron degeneration and induces axonal outgrowth. *Exp Neurol* 1997;144:273–86.
38. Giehl KM, Rohrig S, Bonarz H, et al. Endogenous brain-derived neurotrophic faetor and neurotrophin-3 antagonistically regulate survival of axotomized corticospinal neurons in vivo. *J Neurosci* 2001;21:3492–502.
39. Koda M, Murakami M, Ino H, et al. Brain-derived neurotrophic factor suppresses delayed apoptosis of oligodendrocytes after spinal cord injury in rats. *J Neurotrauma* 2002;19:777–85.
40. Blits B, Boer GJ, Verhaagen J. Pharmacological, cell, and gene therapy strategies to promote spinal cord regeneration. *Cell Transplant* 2002;11:593–613.
41. de Groor DM, Coenen AJ, Verhofstad A, et al. In vivo induetion of glial cell proliferation and axonal outgrowth and myelination by brain-derived neurotrophic factor. *Mol Endocrinol* 2006;20:2987–98.
42. Dasari VR, Spomar DG, Cady C, et al. Mesenchymal stem cells from rat bone marrow downregulate caspase-3-mediated apoptotie pathway afrer spinal cord injury in rats. *Neurochem Res* 2007;32:2080–93.
43. Huang EJ, Reichardt LF. Trk receptors: roles in neuronal signal transduction. *Ann Rev Biochem* 2003;72:609–42.
44. Beattie MS, Harrington AW, Lee R, et al. ProNGF induces p75-mediated dearh of oligodendrocytes following spinal cord injury. *Neuron* 2002;36:375–86.
45. Chu GK, Yu W, Fehlings MG. The p75 neurotrophin receptor is essential for neuronal cell survival and improvement of functional recovery after spinal cord injury. *Neuroscience* 2007;148: 668–82.

46. Keirstead HS, Blakemore WF. Identification of post-mitotic oligodendrocytes incapable of remyelination within the demyelinated adult spinal cord. *J Neuropathol Exp Neurol* 1997;56:1191–201.
47. Polite A, Reynolds R. NG2-expressing cells as oligodendrocyte progenitors expressing in the normal and demyelinated adult central nervous system. *J Anat* 2005;207:707–16.
48. Keirstead HS, Levine JM, Blakemore WF. Response of the oligodendrocyre progenitor cell population (defined by NG2 labelling) to demyelination of rhe adult spinal cord. *Glia* 1998; 22:161–70.
49. Levine JM, Reynolds R. Activation and proliferation of endogenous oligodendroeyte preeursor cells during ethidium bromide-induced demyelinarion. *Exp Neurol* 1999;160:333–47.
50. Van't Veer A, Du Y, Fischer TZ, et al. Brain-derived neurotrophie factor effects on oligodendrocyre progenitors of the basal forebrain are mediated through trkB and the MAP kinase pathway. *J Neurosci Res* 2008;87:69–78.
51. McTiger DM, Horner PJ, Strokes BT, er al. Neurotrophin-3 and brain-derived neurotrophic factor induce oligodendrocyte proliferation and myelination of regenerating axons in the eontused adult rat spinal cord. *J Neurosci* 1998;18:5354–65.

Spine

SPINE Volume 37, Number 11, pp E639–E646

BIOMECHANICS

Cyclic Tensile Strain Facilitates the Ossification of Ligamentum Flavum Through β-Catenin Signaling Pathway

In Vitro Analysis

Hong-Xin Cai, MD,*† Takafumi Yayama, MD, DMSc,* Kenzo Uchida, MD, DMSc,* Hideaki Nakajima, MD, DMSc,* Daisuke Sugita, MD,* Alexander Rodríguez Guerrero, MD,*‡ Ai Yoshida, MD,* and Hisatoshi Baba, MD, DMSc*

Study Design. Histological, immunohistochemical, and real-time reverse transcription-polymerase chain reaction analyses of the expression of cell signaling and transcriptional factors in human ossification of ligamentum flavum (OLF).

Objective. To test the hypothesis that β-catenin plays a role in the ossification of OLF cells in response to cyclic tensile strain.

Summary of Background Data. Several studies have investigated the roles of biomechanical and metabolic factors in the development and progression of OLF, based on the importance of genetic and biological factors. The process of ossification includes enchondral ossification, although such pathology remains poorly defined.

Methods. Using real-time reverse transcription-polymerase chain reaction, we analyzed the mRNA expression levels of signaling factors known to be involved in the ossification process (β-catenin, Runx2, Sox9, and osteopontin) in cultured OLF cells subjected to cyclic tensile strain. Cyclic tensile strain was produced by Flexercell FX-3000 (Flexercell International, Hillsborough, NC), applied for 0, 6, 12, or 24 hours. The localization of these factors was examined in decalcified paraffin OLF sections by immunohistochemistry. Controlled samples were harvested from nonossified ligamentum flavum of patients who underwent thoracic posterior surgical procedures.

Results. Under resting conditions (no tensile strain), the mRNA levels of β-catenin, Runx2, Sox9, and osteopontin in cultured OLF cells were significantly higher than in the control non-OLF cells. Application of cyclic tensile strain to OLF cells resulted in significant increases in mRNA expression levels of β-catenin, Runx2, Sox9, and osteopontin at 24 hours. Hypertrophic chondrocytes present around the calcification front were immunopositive for Runx2 and osteopontin. Immunoreactivity of β-catenin and Sox9 was strongly present in premature chondrocytes in the fibrocartilage area.

Conclusion. Our results indicated that cyclic tensile strain applied to OLF cells activated their ossification through a process mediated by the β-catenin signaling pathway.

Key words: ossification of the ligamentum flavum, cyclic tensile strain, β-catenin signaling, enchondral ossification, chondrocyte differentiation. **Spine 2012;37:E639–E646**

Ossification of ligamentum flavum (OLF) progresses insidiously for a long period of time and could eventually cause devastating and serious spinal cord compromise.[1-3]

OLF with serious spinal cord compromise affects mainly the Japanese population, and only few cases have been reported from Europe, Africa, and East Asian countries.[1-6] The estimated annual rate of surgery for thoracic myelopathy in Japan between 1988 and 1994 was 5.1 per 1 million people; and 64% of these cases were related to OLF.[4] Since Polgär[7] first described the spinal symptoms associated with OLF, several groups have proposed the mechanism involved in the development and progression of OLF[8-11]; however, the exact pathomechanism of OLF and the spatial progress within the spinal canal remains poorly understood, although the importance of certain genetic and biological factors has been acknowledged.

From the *Department of Orthopaedics and Rehabilitation Medicine, Faculty of Medical Sciences, Fukui University, Fukui, Japan; †Department of Orthopedic Surgery, Sir Run Run Shaw Hospital, Zhejiang University School of Medicine, Hangzhou, People's Republic of China; and; ‡Servicio de Neurocirugia, Hospital Nacional Rosales, Universidad de El Salvador, San Salvador, El Salvador.

Acknowledgment date: July 29, 2011. First revision date: November 7, 2011. Acceptance date: November 15, 2011.

The manuscript submitted does not contain information about medical device(s)/drug(s).

The Investigation Committee on Ossification of the Spinal Ligaments and the Public Health Bureau of the Japanese Ministry of Labour, Health and Welfare grants (2004–2010) were received to support this work in part to HB and KU and the Japanese Ministry of Education, Science and Culture grant-in-aid (B18390411, B19791023, C21591895, C21791389, B22390287, and Young-B22791366) to HB, HN, TY, and KU for general scientific research.

No benefits in any form have been or will be received from a commercial party related directly or indirectly to the subject of this manuscript.

Address correspondence and reprint requests to Takafumi Yayama, MD, DMSc, Department of Orthopaedics and Rehabilitation Medicine, Faculty of Medical Sciences, Fukui University, Matsuoka Shimoaizuki 23, Eiheiji, Fukui 910-1193, Japan; E-mail: yayama@u-fukui.ac.jp

DOI: 10.1097/BRS.0b013e318242a132

From a histological point of view, the progression of OLF correlates with enchondral ossification.[12] Structurally, pathological specimens exhibit an ossification front, including a calcified cartilage layer, calcification front, and fibrocartilage layer, between the bone formation and the ligamentous fiber area.[13–15] In our previous study, we reported the abundant presence of chondrocytes in specimens of patients with large-sized ossified plaques, such as fused-type (bilateral ossified plaque fused at midline) or tuberous-type (fused at midline with anterior growth) OLF on computed tomographic axial images.[3] These chondrocytes, especially those around the calcification front, were hypertrophic and secreted growth factors, such as TGF-β, bone morphologic protein, or vascular endothelial growth factor, which probably play a part in the ossification process in an autocrine/paracrine mechanism.[16] Recent reports have emphasized the important roles of signal pathways in enchondral ossification. The Wnt/β-catenin signaling plays a key role in enchondral ossification through the modulation of chondrocyte maturation and hypertrophy during growth plate development.[17,18] However, whether this signaling pathway also plays a role in the process of ossification of spinal ligament is still unknown.

Local environmental factors such as abnormal tensile strain can also contribute to OLF. Examination of surgically resected samples suggests the facilitating role of mechanical axial overload and subsequent increased repetitive tensile strain applied to the thoracic ligamentum flavum on the ossifying process.[19] It has also been suggested that various signaling pathways, including transforming growth factor-β1 (TGF-β1), osteopontin, PGI2/cAMP system, Runx2 and BMP-2, are activated under mechanical stress.[20–23] In this regard, β-catenin signaling, which is involved in the normal physiological response to loading, has a stimulatory role in cellular mechanotransduction and its activation enhances the sensitivity of osteoblasts to mechanical loading.[24]

This study used cultured ligamentum flavum cells under cyclic tensile strain to test the hypothesis that the β-catenin pathway plays a role in mechanotransduction and modulation of chondrocyte and osteoblast differentiation in response to transcription factors. To test the hypothesis, the study focused on the expression and localization of signals that modulate the properties of fibroblasts and chondrocytes during the process of OLF.

PATIENTS AND METHODS

Patient Population

All specimens obtained from 58 patients who presented with progressive symptoms and signs of myelopathy and radiological evidence of OLF and underwent posterior decompression in our department during a period of 15 years were used for histopathological and immunohistochemical analyses. Furthermore, specimens from 6 patients were harvested for cell culture in this study (OLF group; 3 men and 3 women; mean age at surgery, 71.0 yr; range, 59–84 yr). Samples of nonossified ligamentum flavum (non-OLF group), obtained from 6 patients who underwent thoracic posterior surgical procedures for fracture (n = 4) and disc herniation (n = 2), were used as control (4 men and 2 women; mean age, 69.4 yr; range, 52–81 yr). None of the patients had evidence of congenital bone or joint disorders or musculoligamentous tissue abnormalities. Furthermore, none was positive for rheumatoid factor, had hyperparathyroidism, or was being treated with glucocorticoids.

Cell Culture

The cultured ligamentum flavum cells were obtained by the tissue explant method.[22,25] The ligaments were harvested aseptically during surgery, and the surrounding tissues were removed carefully under a dissecting microscope. The ligaments were extirpated carefully from the nonossified areas to avoid contamination with osteogenic cells. The ligaments were minced into approximately 0.5-mm^3 pieces, the fragments were washed and explanted onto 100-mm diameter dish in 10 mL of Dulbecco's Modified Eagle Medium (DMEM) (GIBCO 12320, Low Glucose 1X, Lot 561521, Grand Island, NY) supplemented with 10% fetal bovine serum qualified (GIBCO, Lot 1395965), 1% penicillin/streptomycin (GIBCO 15140, Lot 667553) at 37°C in a humidified atmosphere of 95% air/5% CO_2. The cultures were undisturbed for 48 hours and then the medium was replaced with an equal volume of fresh medium. The cells derived from the explants were harvested from the dishes with 0.02% ethylenediaminetetraacetic acid and 0.05% trypsin for further passages. We used these fibroblast-like cultured cells in this study at the third passage. Microscopic examination showed similar morphology of cultured cells in each passage (spindle-like cells). Furthermore, real-time reverse transcription-polymerase chain reaction (RT-PCR) showed similar mRNA expression levels of collagen type I and transforming growth factor-β1 (TGF-β1) in cells of the first, second, and third passages (data not shown). The samples harvested from 6 patients of the non-OLF group were cultured in a similar fashion.

In Vitro Application of Cyclic Tensile Strain

The cell-stretching device used in this study was a Flexercell FX-3000 strain unit (Flexercell International, Hillsborough, NC). The device consists of a computer-controlled vacuum unit, a flexible bottomed polystyrene culture well plate coated with type I collagen (Flex I, Bioflex Plates; Flexercell International). The culture plates consisted of 6-well (35-mm diameter) flexible bottomed culture plate with a hydrophilic surface. The application of a vacuum provides a hemispherically downward deformation force onto the flexible bottom, resulting in a nonhomogenous strain profile, with a maximum at the periphery and a geometric decline toward zero at the center of the culture well bottom.[26–28] The flexible bottomed culture plates were placed on the vacuum base plate in the incubator (37°C in 5% CO_2). After 3-day cell seeding, the cells were subjected to cyclic tensile strain. On the basis of previous studies,[22,25,29] we set the tensile strain at a maximum 20% elongation. Another reason for the selection was the reported failure strength of strain of 26% in a study using human spinal ligamentum flavum.[30] For this experiment, cultured OLF

TABLE 1. Real-Time Reverse Transcription-Polymerase Chain Reaction Primers Used in This Study

Target Gene	Accession Number	Product Size (bp)	Primer Sequence	
β-*Catenin*	NM_001904.3	122	F	5′-TCTGAGGACAAGCCACAAGATTACA-3′
			R	5′-TGGGCACCAATATCAAGTCCAA-3′
Runx2	NM_001024630.3	127	F	5′-CACTGGCGCTGCAACAAGA-3′
			R	5′-CATTCCGGAGCTCAGCAGAATAA-3′
Sox9	NM_00346.3	82	F	5′-ACCAGTACCCGCACTTGCAC-3′
			R	5′-CGCTTCTCGCTCTCGTTCAG-3′
Osteopontin	NM_001040058.1	115	F	5′-ACACATATGATGGCCGAGGTGA-3′
			R	5′-TGTGAGGTGATGTCCTCGTCTGTAG-3′

F indicates forward primer; R; reverse primer.

cells were subjected to 10-second cycles of 20% elongation and 10 seconds of relaxation for 6, 12, or 24 hours. The cells were observed morphologically, and quantification of mRNA expression of transcription factors after application of cyclic tensile strain was performed.

Measurement of Cell Viability

Cell viability of cultured ligamentum flavum cells was examined by the Live/Dead assay (Cambridge Biosciences, Cambridge, UK) under a confocal microscope (Leica TCS SP2; Wetzlar, Germany). Ethidium homodimer-1 cannot penetrate live cells but stains the DNA of dead cells red. Calcein-AM penetrates live cells where an esterase enzyme cleaves the molecule, which then fluoresces green, whereas dead cells contain no esterase. To visualize, the cells were soaked in the Live/Dead solution for 1 hour. The number of live (green) and dead (red) cells was counted manually.

RT-PCR Analysis

Real-time RT-PCR was used for semiquantitative analysis of the relative mRNA expression levels of transcriptional factors (repeated 3 times for each sample), using 6 cultured OLF samples and 6 non-OLF samples. The cultured cells on each plate were disrupted in a lysis buffer containing β-mercaptoethanol, and the total RNA was purified using RNAiso Plus (code no. 9108/9109; Takara Biomedicals, Ohtsu, Japan) and treated with DNase I (Takara Biomedicals). Reverse transcription was performed using 1 μg of total RNA, PrimeScript RT reagent Kit (code no. RR037A; Takara Biomedicals), and random primer. Real-time RT-PCR was performed on SYBR Premix Ex Taq II (code no. RR081A; Takara Biomedicals), using 1 μL of the synthesized cDNA and SYBR Green PCR master mix (PE Applied Biosystems, Foster City, CA). The primer sequences used in this study are shown in Table 1. The target genes were amplified and analyzed in triplicate, using ABI Prism 7000 SDS Software (Takara Biomedicals). The expression levels of the target genes were estimated relative to that of glyceraldehyde-3-phosphate dehydrogenase (GAPDH). Quality control studies confirmed that cyclic tensile strain applied to both the control and OLF tissues did not significantly change the expression level of GAPDH.

Histopathological and Immunohistochemical Staining

The resected OLF plaque together with the surrounding ligamentum flavum tissue was bisected midsagittally, followed by fixation with 10% buffered formaldehyde for 48 hours at 4°C, decalcified for 4 to 7 days at 4°C in 0.5 M ethylenediaminetetraacetic acid, and 0.5 M Tris-HCl buffer at pH 7.6, and then embedded in paraffin using standard procedures. Serial 4-μm-thick sagittal sections of the OLF were prepared for hematoxylin and eosin, safranin O, and elastica van Gieson staining.

Immunohistochemical processing was performed as described previously.[15,16,31,32] After deparaffinization with xylene, treatment with ethanol, and washing with water, the intrinsic peroxidase was blocked with 0.3% H_2O_2-methanol solution at 20°C for 10 minutes, followed by washing with phosphate-buffered saline (PBS; pH 7.4). The sections were irradiated 3 times with PBS for a period of 5 minutes, using a microwave oven (500 W, ER-245; Toshiba, Tokyo). The sections were then reacted with blocking solution (PBS containing carrier protein and 15 mM of sodium azide; LSAB kit, Lot 00075; Dako, Glostrup, Denmark) at 20°C for 10 minutes. The primary antibodies used in this study were mouse anti-β-catenin (Lot sc-133240; Santa Cruz Biotechnology, Santa Cruz, CA), rabbit polyclonal anti-Runx2 (Lot sc-10758; Santa Cruz Biotechnology), rabbit polyclonal anti-Sox9 (Lot DO406; Santa Cruz Biotechnology), and goat polyclonal anti-osteopontin (Lot sc-10593; Santa Cruz Biotechnology). The sections were further reacted with goat anti-mouse immunoglobulin antibodies conjugated to peroxidase-labeled dextran polymer (EnVision, peroxidase, Dako Corp., Carpentaria, CA) for monoclonal antibodies and with goat anti-rabbit immunoglobulin antibodies (EnVision+, peroxidase, Dako) for polyclonal antibodies at 20°C for 45 minutes and rinsed with PBS at pH 7.4. To visualize the peroxidase color reaction, sections were incubated with DAB-HCl solution (CB090; Dojin Chemicals, Tokyo, Japan; 50 mg dissolved in 100 mL of 0.05 M Tris-HCl buffer at pH 7.4) at

TABLE 2. Cell Survival Rate After Cyclic Tensile Stress*

	0 h	6 h	12 h	24 h
OLF cells	98.3 ± 0.60	96.0 ± 1.38	95.4 ± 1.88	92.4 ± 2.35
Non-OLF cells	97.8 ± 0.51	96.2 ± 1.26	94.0 ± 1.15	90.4 ± 2.90

*Values given are mean ± SD.

OLF indicates ossification of ligamentum flavum.

20°C for 10 minutes. Nuclear counterstaining was carried out with hematoxylin.

Statistical Analysis

Data were expressed as mean ± SEM. Differences between groups were examined by the Student *t* test. A *P* value of less than 5% was considered significant.

RESULTS

Cultured Cell Morphology

The cultured ligamentum flavum cells exhibited a fibroblast-like, spindle-shaped appearance. The viability of the attached OLF cells was 92.4% ± 2.35% and 90.4% ± 2.90% in 24-hour cyclic tensile strain and nonstrain experiments, respectively (Table 2; also see Supplementary Data 1, Supplementary Digital Content 1, available at: http://links.lww.com/BRS/A594). At each time point, the viability of stressed OLF cells was not significantly different from that of non-OLF cells.

Real-Time RT-PCR and Immunohistochemistry of Cultured Ligamentum Flavum Cells

Figure 1 shows the relative mRNA expression levels in OLF cells, using real-time RT-PCR analysis. Under no-stress condition, the mRNA expression levels of β-catenin (Figure 1A), Runx2 (Figure 1B), Sox9 (Figure 1C), and osteopontin (Figure 1D) were significantly higher in OLF cells than in non-OLF cells (see Supplementary Data 2, Supplemental Digital Content 2, available at: http://links.lww.com/BRS/A595). Application of cyclic tensile strain to OLF samples resulted in significant increases in mRNA expression levels of β-catenin and Sox9 at 6 to 12 hours and Runx2 and osteopontin at 24 hours. In the control samples, application of cyclic tensile strain significantly increased the mRNA expression levels of Sox9 but not those of β-catenin, Runx2, and osteopontin.

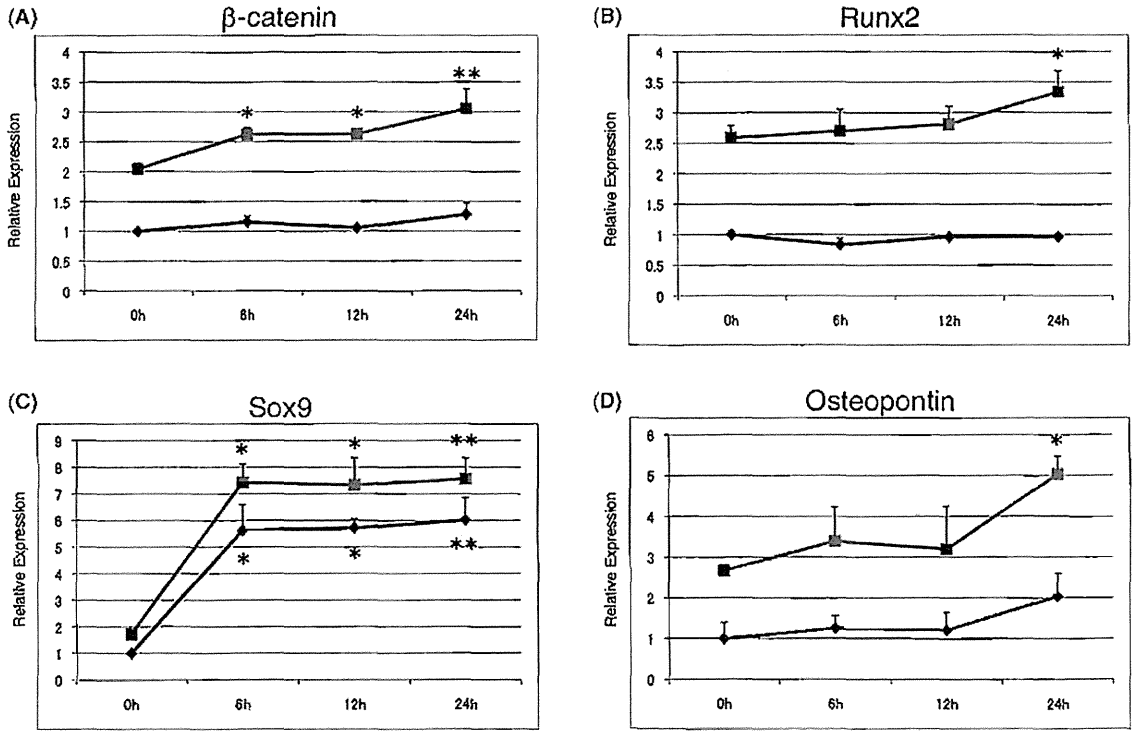

Figure 1. Real-time reverse transcription-polymerase chain reaction analysis of ossification of ligamentum flavum (OLF) (red line) and non-OLF (blue line) cultured ligament cells. Relative mRNA expression levels of (**A**) β-catenin, (**B**) Runx2, (**C**) Sox9, and (**D**) osteopontin increased significantly after the application of tensile strain in OLF cells. In control cells, cyclic tensile strain did not change the expression of β-catenin, Runx2, or osteopontin. *$P < 0.05$, **$P < 0.01$, compared with each value at 0 hour.

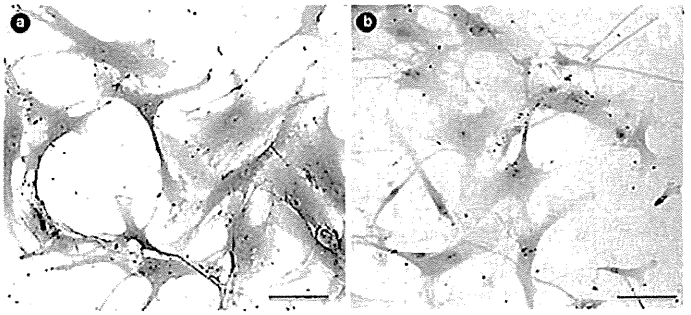

Figure 2. Immunohistochemical examination showing positively stained cultured ossification of ligamentum flavum cells. (A), Representative case (positive staining for β-catenin). (B), Negative control scale bar = 100 μm.

Immunohistochemically, cultured ligamentum flavum cells derived from OLF samples were immunopositive for β-catenin, Runx2, Sox9, and osteopontin under mechanical stress (Figure 2A). On the contrary, non-OLF cells showed no immunoreactivity for β-catenin, Runx2, Sox9, and osteopontin without strain but became positive for Sox9 after tensile strain application (Figure 2B).

Histopathological and Immunohistochemical Findings of Paraffin Sections

In non-OLF samples, a thin-layered structure was identified between the fiber area and the laminar bone, and the elastic fibers showed uniform arrangement extending into the bony attachment. In OLF samples, the ossification fronts, including the fibrocartilage layer, calcification front, and the calcified cartilage layer, were wider showing significant irregularities with several disruptions. A significant number of chondrocytes were present at the ossification front, particularly around the calcification front. The elastic fibers showed irregular arrangement and abnormally fragmented elastic fibers of small diameter (Figure 3).

The hypertrophic chondrocytes present around calcification front were immunopositive for Runx2 and osteopontin but negative for β-catenin and Sox9, and strong immunoreactivity to β-catenin and Sox9 was noted in premature chondrocytes in the fibrocartilage area. On the contrary, β-catenin and Sox9 expression levels were significant in mesenchymal cells present around the ossification front, where the ligamentous matrix showed degenerative changes in these patients (Figure 4, Table 3).

DISCUSSION

The current study characterized the distribution and expression levels of various signal transduction factors involved in the process of ossification of the thoracic ligamentum flavum. The main findings of our study were as follows: (1) cultured ligamentum flavum cells from OLF samples overexpressed β-catenin, Runx2, Sox9, and osteopontin compared with control non-OLF samples; (2) cyclic tensile strain applied for 24 hours increased the mRNA expression levels of β-catenin, Runx2, Sox9, and osteopontin in OLF cells, whereas similar mechanical stress produced negligible changes in the mRNA expression of β-catenin, Runx2, and osteopontin in non-OLF cells; and (3) immunoreactivity for β-catenin and Sox9 was noted in premature chondrocytes, and immunostaining for Runx2 and osteopontin was strongly positive in hypertrophic chondrocytes around the calcification front.

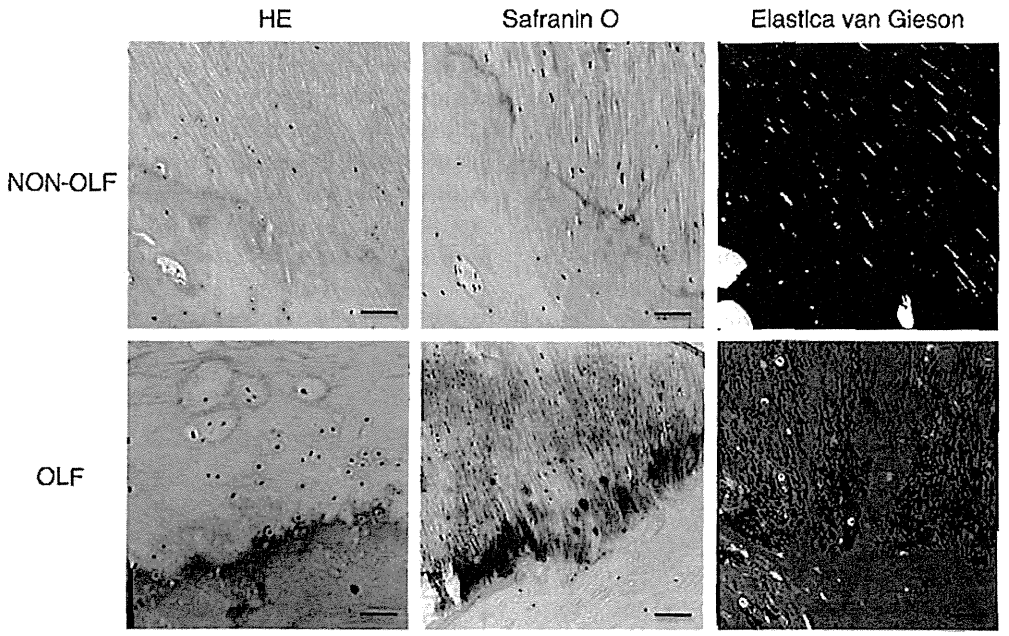

Figure 3. Histopathological examination showing the presence of a thin-layered structure between the fibers and the laminar bone. The elastic fibers show uniform arrangement extending to the ligamentous enthesis in non-OLF cells. In the OLF sample, note the wider bundles of elastic fibers, with significant irregularities and several disruptions. Also note the significant number of chondrocytes at the ossification front, particularly around the calcification front (scale bar = 100 μm). HE indicates hematoxylin-eosin; Non-OLF, nonossified ligamentum flavum; OLF, ossification of ligamentum flavum.

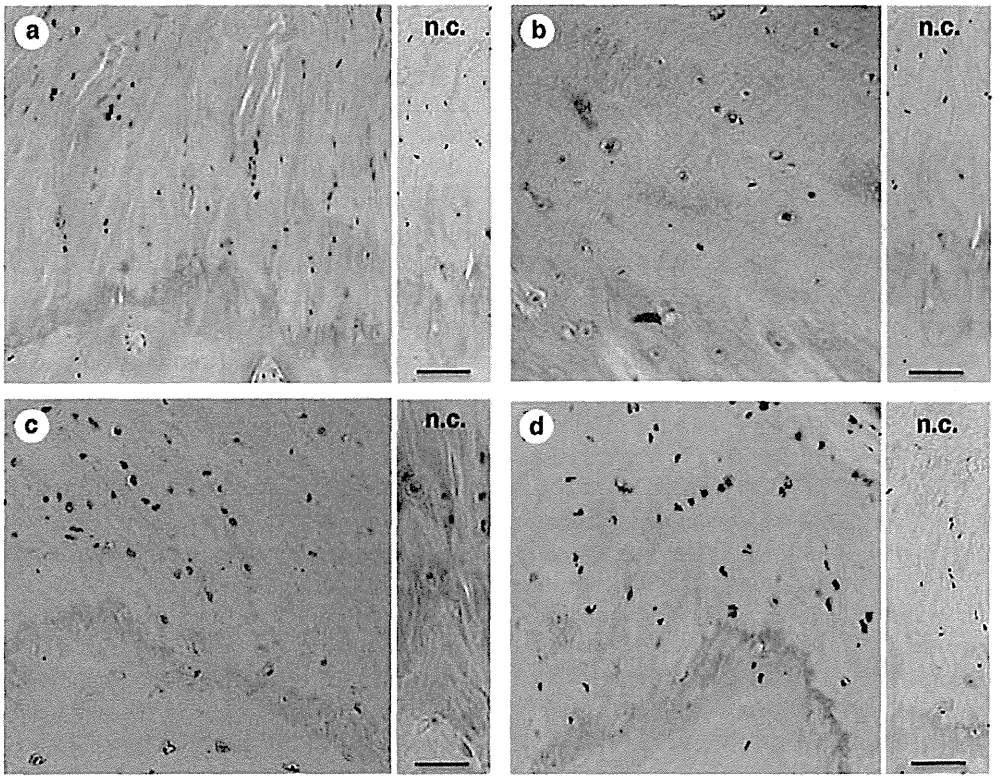

Figure 4. *Immunohistochemical analysis of β-catenin (A), Runx2 (B), Sox9 (C), and osteopontin (D). The hypertrophic chondrocytes were positive for Runx2 and osteopontin. The immunoreactivities of β-catenin and Sox9 were strong in premature chondrocytes in the fibrocartilage area. NC indicates negative control. Scale bar = 100 μm.*

Several studies have discussed the possible roles of mechanical, metabolic, genetic, and cellular factors in the development and progression of OLF. At the genetic level, previous studies identified abnormalities in *COL6A2* and *COL11A1* genes on chromosome 6p21 and chromosome 21p22.3, respectively, in patients with ossification of the spinal ligaments, suggesting that these genetic abnormalities might explain the diversity of biological properties in OLF cells.[11,33] Furthermore, we have demonstrated, for the first time, the upregulation of β-catenin, Runx2, Sox9, and osteopontin mRNA levels in cultured OLF cells. Considered together, these results suggest that cultured OLF cells have unique cell properties compared with non-OLF cells and can possibly respond to genetic, environmental, and/or biological factors in a manner different from that of non-OLF cells.

The ligamentum flavum is persistently subjected to distraction strain along its longitudinal axis, as well as large mechanical overload, and such mechanical stress contributes to the ossification process. In the histopathological study, elastic fibers displayed irregular arrangement associated with the degeneration process compared with the normal ligamentum flavum with regular arrangement of elastic fiber bundles.[34] Previous studies analyzed the degenerative changes by quantifying the decrement in elastic fibers, increment in collagen fibers, and changes in the expanding chondrometaplastic areas in the degenerated ligament.[35,36] Studies from our group also demonstrated the disappearance of the normal arrangement of elastic fibers after expansion of fibrosis as well as the presence of chondrometaplastic areas at the ossification front, especially in large ossified plaques, such as fused- or tuberous-type OLF cells.[16,37] We think that these degenerative changes are followed by the ossification process and mechanical stress contributes to the loss of normal ligament arrangement. In addition, previous studies reported that repetitive distraction strain could change the sensitivity of spinal ligament cells through the modulation of their osteogenic properties, such as the expression of osteopontin, resulting in initiation and development of ossification.[8,9,38] Our results also demonstrated that cyclic tensile strain altered

TABLE 3. Immunohistochemical Localization in the Ossification Front

	Ossified Area	Calcified Cartilage Layer	Fibrocartilage Layer	Fiber Area
β-Catenin	−	+	++	−
Runx2	−	+	+	−
Sox9	−	−	++	±
Osteopontin	±	+	+	−

++ indicates strongly positive; +, moderately positive; ±, weakly positive; −, negative staining, semiquantitative analysis conducted according to the method described by Kokubo et al[31] and Song et al.[32]

the upregulation of signaling and transcriptional factors secreted by cultured OLF cells.

The progression of OLF correlates with enchondral ossification, which is also an important process in the development of the growth plate. During enchondral ossification, regulation of chondrocyte differentiation is the most important factor for osteoblast differentiation and maturation under the influence of growth and transcriptional factors.[12,39] The Wnt/β-catenin signaling regulates chondrocyte phenotype, maturation, and function in a developmentally regulated manner, and the regulated action of this pathway is critical for growth plate organization, cartilage boundary definition, and enchondral ossification.[17,20,40] Upregulation of this signaling pathway could accelerate chondrocyte maturation, which regulates the initiation of chondrocyte hypertrophy and also controls the final maturation of hypertrophic chondrocytes, suggesting cooperation with Runx2, Sox9, and/or other transcriptional factors.[41–44] Using an animal model, Yuasa *et al*[18] reported that transient activation of the Wnt/β-catenin signaling pathway induces abnormal closure of the growth plate and thickening of the articular cartilage. Considered together, our results suggest that cyclic tensile strain induces overexpression of β-catenin signaling, resulting in upregulation of transcriptional factors, growth factors, and/or cytokines, during the enchondral ossification process in OLF.

In conclusion, chondrocyte differentiation leading to enchondral ossification in OLF is regulated by signal transduction, such as β-catenin, and transcriptional factors. These factors were overexpressed in cultured OLF cells, suggesting genetic control of this process. The mRNA expression levels of transcriptional factors and β-catenin signaling were higher under mechanical stress, indicating that transient activation of β-catenin signaling is an important process in the ossification process in OLF. Although the duration of the cyclic tensile stress applied to cultured cells is shorter than that in the *in vivo* environment, we think that such stress is an important factor in the initiation of the ossification process. Further studies are needed to investigate the relationship between mechanical force and the expression of various signal transductions in OLF.

This study has certain limitations. We conducted studies of the cellular responses in cultured cells maintained *in vitro*, and the findings cannot be extrapolated with certainty to human where cells are surrounded by the extra-cellular matrix. Furthermore, although the duration of the cyclic tensile strain applied to cultured cells was shorter than that *in vivo*, we think that such strain is an important factor in the initiation of the ossification process. Further studies are needed to investigate the relationship between mechanical force and the expression of various signal transduction factors in OLF.

In conclusion, chondrocyte differentiation with subsequent enchondral ossification in OLF is regulated by the expression of signal transduction and/or transcriptional factors. The mRNA expression levels of transcriptional factors and β-catenin signaling were higher under mechanical stress, indicating that transient activation of β-catenin signaling is an important process in the OLF ossification process.

➢ Key Points

- ❑ In OLF samples, the ossification front contained numerous chondrocytes and abnormally arranged elastic fiber bundles.
- ❑ OLF samples contained premature chondrocytes immunostained for β-catenin and Sox9, whereas hypertrophic chondrocytes around the calcification front immunostained strongly for Runx2 and osteopontin.
- ❑ Cultured ligamentum flavum cells derived from surgical specimens of patients with OLF expressed high levels of β-catenin, Runx2, Sox9, and osteopontin mRNAs, compared with non-OLF samples.
- ❑ Cyclic tensile strain applied for 24 hours to cultured cells upregulated the expression levels of β-catenin, Runx2, Sox9, and osteopontin in OLF cells but had little effect on β-catenin, Runx2 and osteopontin mRNAs in non-OLF cells.

Supplemental digital contents are available for this article. Direct URL citations appear in the printed text and are provided in the HTML and PDF versions of this article on the journal's Web site (www. spinejournal.org).

References

1. Baba H, Tomita K, Maezawa Y, et al. Intermittent claudication of the spinal cord due to ossification of the ligamentum flavum. A report of two cases. *Int Orthop* 1993;17:169–72.
2. Guo JJ, Luk KD, Karppinen J, et al. Prevalence, distribution, and morphology of ossification of the ligamentum flavum: a population study of one thousand seven hundred thirty-six magnetic resonance imaging scans. *Spine* 2010;35:51–6.
3. Miyakoshi N, Shimada Y, Suzuki T, et al. Factors related to long-term outcome after decompressive surgery for ossification of the ligamentum flavum of the thoracic spine. *J Neurosurg* 2003;99(suppl 3):251–6.
4. Sato T, Kokubun S, Tanaka Y, et al. Thoracic myelopathy in the Japanese: epidemiological and clinical observations on the cases in Miyagi Prefecture. *Tohoku J Exp Med* 1998;184:1–11.
5. Pascal-Mousselard H, Smadja D, Cabre P, et al. Ossification of the ligamenta flava with severe myelopathy in a black patient. A case report. *Spine* 1998;23:1607–8.
6. Arafat QW, Jackowski A, Chavda SV, et al. Case report: ossification of the thoracic ligamenta flava in a Caucasian: a rare cause of myelopathy. *Br J Radiol* 1993;66:1193–6.
7. Polgär F. Über interarknelle wirbelverkalkung. *Fortschr Geb Rontgenstr Nuklearmed Ergänzungsband.* 1920;40:292–8.
8. Iwamoto Y, Tsukamoto N, Maeda K, et al. *Effects of Repetitive Distraction Stress on Rat Spinal Ligaments: In Vivo Cell Biological Study.* Annual Report of Researches on Ossification of the Spinal Ligament. Tokyo, Japan: The University of Tokyo; 2006: 65–70.
9. Tsukamoto N, Maeda T, Miura H, et al. Repetitive tensile stress to rat caudal vertebrae inducing cartilage formation in the spinal ligaments: a possible role of mechanical stress in the development of ossification of the spinal ligaments. *J Neurosurg Spine* 2006;5: 234–42.
10. Inamasu J, Guiot BH, Sachs DC. Ossification of the posterior longitudinal ligament: an update on its biology, epidemiology, and natural history. *Neurosurgery* 2006;58:1027–39.
11. Tanaka T, Ikari K, Furushima K, et al. Genomewide linkage and linkage disequilibrium analyses identify COL6A1, on chromosome 21, as the locus for ossification of the posterior longitudinal ligament of the spine. *Am J Hum Genet* 2003;73:812–22.

12. Miyasaka K, Kaneda K, Sato S, et al. Myelopathy due to ossification or calcification of the ligamentum flavum: radiologic and histologic evaluations. *AJNR Am J Neuroradiol* 1983;4:629–32.
13. Okada K, Oka S, Tohge K, et al. Thoracic myelopathy caused by ossification of the ligamentum flavum. Clinicopathologic study and surgical treatment. *Spine* 1991;16:280–7.
14. BenHamouda K, Jemel H, Haouet S, et al. Thoracic myclopathy caused by ossification of the ligamentum flavum: a report of 18 cases. *J Neurosurg* 2003;99:157–61.
15. Sato R, Uchida K, Kobayashi S, et al. Ossification of the posterior longitudinal ligament of the cervical spine: histopathological findings around the calcification and ossification front. *J Neurosurg Spine* 2007;7:174–83.
16. Yayama T, Uchida K, Kobayashi S, et al. Thoracic ossification of the human ligamentum flavum: histopathological and immunohistochemical findings around the ossified lesion. *J Neurosurg Spine* 2007;7:184–93.
17. Day TF, Yang Y. Wnt and Hedgehog signaling pathways in bone development. *J Bone Joint Surg Am* 2008;90:19–24.
18. Yuasa T, Kondo N, Yasuhara R, et al. Transient activation of Wnt/β-carenin signaling induces abnormal growth plate closure and arricular cartilage thickening in postnatal mice. *Am J Pathol* 2009;175:1993–2003.
19. Li F, Chen Q, Xu K. Surgical treatment of 40 patients with thoracic ossification of the ligamentum flavum. *J Neurosurg Spine* 2006;4:191–7.
20. Tamamura Y, Otani T, Kanatani N, et al. Developmental regulation of Wnt/β-catenin signals is required for growth plate assembly, cartilage integrity, and endochondral ossification. *J Biol Chem* 2005;280:19185–95.
21. Wu Q, Chen D, Zuscik MJ, et al. Overexpression of Smurf2 stimulates endochondral ossification through upregulation of β-carenin. *J Bone Miner Res* 2008;23:552–63.
22. Iwasaki K, Furukawa KI, Tanno M, et al. Uni-axial cyclic stretch induces Cbfa1 expression in spinal ligament cells derived from patients with ossification of the posterior longitudinal ligament. *Calcif Tissue Int* 2004;74:448–57.
23. Sen B, Xie Z, Case N, et al. Mechanical strain inhibits adipogenesis in mesenchymal stem cells by stimulating a durable β-catenin signal. *Endocrinology* 2008;149:6065–75.
24. Case N, Ma M, Sen B, et al. β-Catenin levels influence rapid mechanical responses in osteoblasts. *J Biol Chem* 2008;283:29196–205.
25. Ohishi H, Furukawa K, Iwasaki K, et al. Role of prostaglandin I_2 in the gene expression induced by mechanical stress in spinal ligament cells derived from patients with ossification of the posterior longitudinal ligament. *J Pharmacol Exp Ther* 2003;305:818–24.
26. Nakatani T, Marui T, Hitora T, et al. Mechanical stretching force promotes collagen synthesis by cultured cells from human ligamentum flavum via transforming growth factor-β1. *J Orthop Res* 2002;20:1380–6.
27. Banes AJ, Gilbert J, Taylor D, et al. A new vacuum-operated stress-providing instrument that applies static or variable duration cyclic tension or compression to cells in vitro. *J Cell Sci* 1985;75:35–42.
28. Gilbert JA, Weinhold PS, Banes AJ, et al. Strain profiles for circular cell culture plates containing flexible surfaces employed to mechanically deform cells in vitro. *J Biomech* 1994;27:1169–77.
29. Uchida K, Nakajima H, Takamura T, et al. Gene expression profiles of neurotrophic factors in rat cultured spinal cord cells under cyclic tensile stress. *Spine* 2008;33:2596–604.
30. White AA, Panjabi MM. *Clinical Biomechanics of the Spine*. 2nd ed. Philadelphia: JB Lippincott Company; 1990.
31. Kokubo Y, Kobayashi S, Uchida K, et al. Herniated and spondylotic intervertebral discs of the human cervical spine: histological and immunohistochemical observations. *Acta Histochem Cytochem* 2004;37:109–17.
32. Song J, Mizuno J, Hashizume Y, et al. Immunohistochemistry of symptomatic hypertrophy of the posterior longitudinal ligament with special reference to ligamentous ossification. *Spinal Cord* 2006;44:576–81.
33. Kong Q, Ma X, Li F, et al. COL6A1 polymorphisms associated with ossification of the ligamentum flavum and ossification of the posterior longitudinal ligament. *Spine* 2007;32:2834–8.
34. Yoshida M, Shima K, Taniguchi Y, et al. Hypertrophied ligamentum flavum in lumbar spinal canal stenosis. Pathogenesis and morphologic and immunohistochemical observation. *Spine* 1992;17:1353–60.
35. Kashiwagi K. Histological changes of the lumbar ligamentum flavum with aging (abstract in English). *J Jpn Orthop Assoc* 1993;67:221–9.
36. Schräder PK, Grob D, Rahn BA, et al. Histology of the ligamentum flavum in patients with degenerative lumbar spinal stenosis. *Eur Spine J* 1999;8:323–8.
37. Yayama T, Baba H, Furusawa N, et al. Pathogenesis of calcium crystal deposition in the ligamentum flavum correlates with lumbar spinal canal stenosis. *Clin Exp Rheumatol* 2005;23:637–43.
38. Zuscik MJ, Hilton MJ, Zhang X, et al. Regulation of chondrogenesis and chondrocyte differentiation by stress. *J Clin Invest* 2008;118:429–38.
39. Goldring MB, Tsuchimochi K, Ijiri K. The control of chondrogenesis. *J Cell Biochem* 2006;97:33–44.
40. Andrade AC, Nilsson O, Barnes KM, et al. Wnt gene expression in the post-natal growth plate: regulation with chondrocyte differentiation. *Bone* 2007;40:1361–9.
41. Guo X, Mak KK, Taketo MM, et al. The Wnt/β-catenin pathway interacts differentially with PTHrP signaling to control chondrocyte hypertrophy and final maturation. *PLoS One* 2009;4:e6067.
42. Dong YF, Soung DY, Schwarz EM, et al. Wnt induction of chondrocyte hypertrophy through the Runx2 transcription factor. *J Cell Physiol* 2006;208:77–86.
43. Fan D, Chen Z, Wang D, et al. Osterix is a key target for mechanical signals in human thoracic ligament flavum cells. *J Cell Physiol* 2007;211:577–84.
44. Robinson JA, Chatterjee-Kishore M, Yaworsky PJ, et al. Wnt/β-catenin signaling is a normal physiological response to mechanical loading in bone. *J Biol Chem* 2006;281:31720–8.

Anal Bioanal Chem (2012) 403:1873–1884
DOI 10.1007/s00216-012-5900-3

ORIGINAL PAPER

Spatiotemporal alteration of phospholipids and prostaglandins in a rat model of spinal cord injury

Mitsuru Hanada · Yuki Sugiura · Ryuichi Shinjo · Noritaka Masaki · Shiro Imagama · Naoki Ishiguro · Yukihiro Matsuyama · Mitsutoshi Setou

Received: 22 November 2011 / Revised: 27 January 2012 / Accepted: 24 February 2012 / Published online: 14 March 2012

Abstract We determined quantitative and qualitative alterations in lipids during the occurrence and progression of spinal cord injury (SCI) in rats to identify potential clinical indicators of SCI pathology. Imaging mass spectrometry (IMS) was used to visualize twelve molecular species of phosphatidylcholine (PC) on thin slices of spinal cord with SCI. In addition, twelve species of phospholipids and five species of prostaglandins (PGs) were quantified by liquid chromatography–electrospray ionization–tandem mass spectrometry (LC-ESI-MS/MS) of lipid extracts from control/injured spinal cords. Unique distribution patterns were observed for phospholipids with different fatty acid compositions, and distinct dynamic changes were seen in both their amounts and their distributions in tissue as tissue damage resulting from SCI progressed. In particular, PCs containing docosahexaenoic acid localized to the large nucleus in the anterior horn region at one day post-SCI and rapidly decreased thereafter. In contrast, PCs containing arachidonic acid (AA-PCs) were normally found in the posterior horn region and were intensely and temporarily elevated one week after SCI. Lysophosphatidylcholines (LPCs) also increased at the same SCI stage and in regions with elevated AA-PCs, indicating the release of AA and the production of PGs. Moreover, LC-ESI-MS/MS analysis of lipid extracts from the spinal cord tissue at the impact site demonstrated a peak in PGE2 that reflected the elevation/reduction pattern of AA-PCs and LPC. Although further investigation is required, we suggest that invasive immune cells that penetrated from the impaired blood–brain barrier at 1–2 weeks post-SCI may have produced LPCs, released AA from AA-PCs, and produced PGs in SCI tissue at sites enriched in AA-PCs/LPC.

Keywords Imaging mass spectrometry · LC-ESI-MS/MS · Phospholipids · Prostaglandins · Spinal cord injury

Mitsuru Hanada and Yuki Sugiura contributed equally to this work.

Published in the special paper collection *Biomedical Mass Spectrometry* with guest editors Toyofumi Nakanishi and Mitsutoshi Setou.

Electronic supplementary material The online version of this article (doi:10.1007/s00216-012-5900-3) contains supplementary material, which is available to authorized users.

M. Hanada · Y. Matsuyama
Department of Orthopaedic Surgery,
Hamamatsu University School of Medicine,
Handayama 1-20-1,
Hamamatsu, Shizuoka 431-3192, Japan

Y. Sugiura
Precursory Research for Embryonic Science and Technology (PRESTO), Japan Science and Technology Agency (JST),
3-5 Sanban-cho,
Chiyoda-ku, Tokyo 102-0075, Japan

N. Masaki · M. Setou (✉)
Department of Molecular Anatomy,
Hamamatsu University School of Medicine,
Handayama 1-20-1,
Hamamatsu, Shizuoka 431-3192, Japan
e-mail: mitsutoshi.setou@gmail.com

M. Setou
e-mail: setou@hama-med.ac.jp

R. Shinjo · S. Imagama · N. Ishiguro
Department of Orthopedics,
Nagoya University Graduate School of Medicine,
Nagoya 466-8550, Japan

Introduction

Lipids are the most common biomolecules found in the central nervous system (CNS), including the spinal cord, and comprise up to half its dry weight [1]. Diverse types of lipids play fundamental roles in cellular functions of the CNS, particularly

in regulating the physical properties of cellular membranes [1–5] and in transmitting signals via the production of bioactive lipids such as prostaglandins (PGs) [1, 6, 7]. Alterations in lipid metabolism may play an important role in neurological disorders and CNS injury. Indeed, levels of several lipids are strongly correlated with the occurrence and progression of tissue disorganization due to spinal cord injury (SCI), which results from an initial trauma followed by a degenerative process. Severe inflammation found in injured spinal cord [8, 9] was associated with bioactive lipids, including PGs produced by invasive immune cells. Similarly, elevated levels of the lysophospholipid group in SCI were also observed [10, 11], highlighting the importance of lipid dynamics in tissue inflammation [10–13].

Lipid research has traditionally focused on the biochemical quantification of lipids in fluid samples of cellular or tissue extracts to elucidate numerous physiologically important roles of lipids. However, the emerging lipid molecular imaging technology, imaging mass spectrometry (IMS) allows spatially resolved imaging of lipids, and provides qualitative information on lipid distribution in situ [14]. Furthermore, the integration of quantitative techniques [e.g., liquid chromatography or gas chromatography coupled to MS or tandem mass spectrometry (MS/MS)] with qualitative methods such as IMS provides researchers with the tools needed to quantify the amount of lipid molecules produced by specific cells in situ.

In particular, IMS incorporating matrix-assisted laser desorption/ionization (MALDI) is a powerful and practical tool in lipid research [10, 14–17]. The unique advantages of IMS include the following: (i) simultaneous detection of multiple lipids in the same specimen, which has shown that slight structural differences in lipid molecules produce a heterogeneous distribution pattern in biological tissues [13, 14, 18–20]; (ii) application to a wide range of analytes [21], ranging from small and simple to large and more complex lipids such as glycolipids with complex oligosaccharide moieties [22, 23]; (iii) a simple and fast protocol [17]. In fact, using SCI model rats, a recent study by Cooks' group found that specific lipid species accumulated in the lesion epicenter and adjacent areas after SCI [13].

The introduction of IMS into classical lipid research is a frontier issue because, both qualitative and quantitative analyses are necessary in medical/biological research in order to understand complex biological phenomena and their regulation (i.e., the regulation of local concentrations of biomolecules in subcellular organelles up to the tissue substructure level). RNAs are routinely localized using in situ hybridization and quantitative real-time PCR with oligonucleotide probes, whereas proteins are localized by immunostaining methods and quantified by western blotting with antibodies. In this context, we and other groups have integrated MALDI-IMS with liquid chromatography–electrospray ionization–MS/MS (LC-ESI-MS/MS) in order to identify specific tissue regions or the cellular production of specific lipids in situ [18, 24]. However, given the complex nature of biological tissue samples that have not been subjected to analyte purification, numerous competing endogenous ion peaks are present in each spectrum acquired by MALDI-IMS. Both LC-resolved lipid identification (based on MS/MS scanning data) [26] and quantification data (based on multiple reaction monitoring [MRM] data) [25, 27] can enhance the data obtained by IMS.

Therefore, an improved understanding of the molecular mechanism of lipid pathophysiology involved in SCI may be achieved through the integrated use of qualitative and quantitative lipid analyses, which may also lead to the discovery of efficient therapies. The aim of the present study was to quantitatively and qualitatively examine alterations in lipids during the occurrence and progression of SCI in order to identify potential clinical indicators that may be used to evaluate SCI pathology.

Materials and methods

Chemicals

Methanol, potassium acetate, and ultrapure water were purchased from Wako Chemicals (Osaka, Japan). Calibration-standard peptide and 2,5-dihydroxybenzoic acid (DHB) were purchased from Bruker Daltonics (Leipzig, Germany), and 9-aminoacridine was purchased from Acronics (Pittsburgh, PA, USA). All of the chemicals used in this study were of the highest purity available.

Abbreviations for glycerophospholipids

The structures of the side chains of gycerophospholipid species with one or two radyl side chains are indicated within parentheses in the "headgroup(coupling scheme/sn1/sn2)" format [e.g., PC(diacyl-16:0/18:1)].

Animals

All experiments were performed according to the guidelines for animal experimentation and the care and use of laboratory animals established by Nagoya University School. Nine-week-old Sprague–Dawley rats (190–210 g) were used in this study.

Generation of SCI rats

All rats were deeply anesthetized with 25 mg/kg pentobarbital sodium. Laminectomy was performed at the ninth and tenth thoracic (T10) levels, and contusion injury of the spinal cord was introduced at level T10 using the Infinite Horizon impactor (IH impactor, 200 kdyn; Precision Systems and Instrumentation, Lexington, NY, USA). After contusion injury, the laminectomy was closed by suturing the muscle with nylon, followed by the

use of wound clips to close the skin incision site. Rats with SCI at the site of injury were sacrificed 12 h (hours); 1 d (day); or 1, 2, or 8 w (weeks) post-SCI.

Tissue preparation

Rats were anesthetized with 25 mg/kg pentobarbital sodium and sacrificed by transcardial perfusion with cold PBS, and the spinal cords of rats with SCI were extracted (approximately 2 cm in length around the SCI). Similarly, the spinal cords of rats without SCI were also extracted (approximately 2 cm in length around the T10-level cord). Immediately after dissection, the spinal cords were flash frozen in dry ice and stored in a deep freezer at −80 °C. Spinal cord tissues were divided into four sections of thickness 5 mm from the proximal to the distal side of the SCI site.

Overall experimental procedure

An outline of the experimental procedure employing MALDI-IMS and LC-ESI-MS/MS to analyze alterations in the lipids in the spinal cords of rats with SCI is shown inFig. S1 of the "Electronic supplementary material" (ESM) . Dissected rat spinal cords with/without SCI treatment were sectioned into four tissue blocks (from the proximal to the distal side) and stored at −80 °C until further use. For IMS, each frozen block was thinly sliced in a cryo-chamber, and the residual blocks were used for LC-ESI-MS/MS. Spatial alterations of lipids between different tissue locations and time points after SCI were explored by IMS. The relative abundance of phospholipids and the absolute abundance of PGs in lipid extracts from tissue blocks were quantified by LC-ESI-MS/MS.

IMS sample preparation

The 5 mm tissue sections were sliced to a thickness of 8 μm with a cryostat (CM1950; Leica, Wetzler, Germany), placed directly onto MALDI plate inserts, and stored at 20 °C until matrix application and subsequent IMS analysis.

Spray coating of the matrix solution for IMS

A DHB solution (40 mg/mL DHB, 20 mM potassium acetate, 70% MetOH, and 0.1% TFA) was used as the matrix solution to image phosphatidylcholine (PC). The matrix solution (approximately 100 μL) was sprayed over the tissue surface using a 0.2 mm nozzle caliber airbrush (Procon Boy FWA Platinum; Mr. Hobby, Tokyo, Japan). Tissue sections for comparison were simultaneously spray coated with each matrix solution to equalize analyte the extraction and co-crystallization conditions. The distance between the nozzle tip and the tissue surface was 10 cm, and the spraying period was fixed at 5 min.

IMS conditions

Single MS imaging was performed using a MALDI TOF/TOF-type instrument (Ultraflex 2 TOF/TOF; Bruker Daltonics) equipped with a 355 nm Nd:YAG laser. The data were acquired in the positive reflectron mode under an accelerating potential of 20 kV using an external calibration method. Signals between *m/z* 400 and 1,000 were collected. Raster scans on tissue surfaces were performed automatically using the FlexControl and FlexImaging 2.0 software (Bruker Daltonics). The number of laser irradiations was 200 shots at each spot. Image reconstruction was performed with the FlexImaging 2.0 software.

LC-ESI-MS/MS

ESI-MS/MS analysis was performed using a 4000Q-TRAP quadrupole linear ion trap hybrid mass spectrometer (Applied Biosystems/MDS Sciex, Concord, ON, Canada) with an Acquity Ultra Performance LC (Waters, Milford, MA, USA). A chromatographic method was developed using an Acquity UPLCTM BEH C18 column (2.1×50 mm i.d., 1.7 μm particles) fitted with an identically packed guard column (2.1× 5 mm; Waters). The column oven was maintained at 40 °C. A gradient elution with mobile phase A [acetonitrile:methanol: water, 19:19:2 (v/v/v) containing 0.1% formic acid and 0.028% ammonia] and mobile phase B (isopropanol, 0.1% formic acid, and 0.028% ammonia) was used at a flow rate of 0.4 mL/min: 0–10 min: 5% B → 5% B; 10–15 min: 5% B → 50% B; 15–20 min: 50% B → 5% B; and 20–25 min: 5% B.

Quantification of PGs

PGs in the spinal cords were quantified as described by the method of Kita et al. [28]. Briefly, the triple quadrupole mass spectrometer equipped with an ESI ion source (4000-Qtrap) was operated in negative ESI and MRM mode. For accurate quantification, an internal standard method was used that employed a mixture of deuterium-labeled PG as an internal standard.

Results and discussion

Characteristic distribution of PC molecular species in normal spinal cords

IMS analysis of the spinal cord tissue of all rats revealed characteristic PC distribution patterns that depended on fatty acid composition, which reflected the heterogeneous membrane lipid compositions of distinct cell types. As shown in Fig. 1a, phospholipids in normal spinal cord sections were examined by MALDI-IMS in the positive ion detection mode. As a result, approximately 150 mass peaks in the mass range of 700<*m/z*<

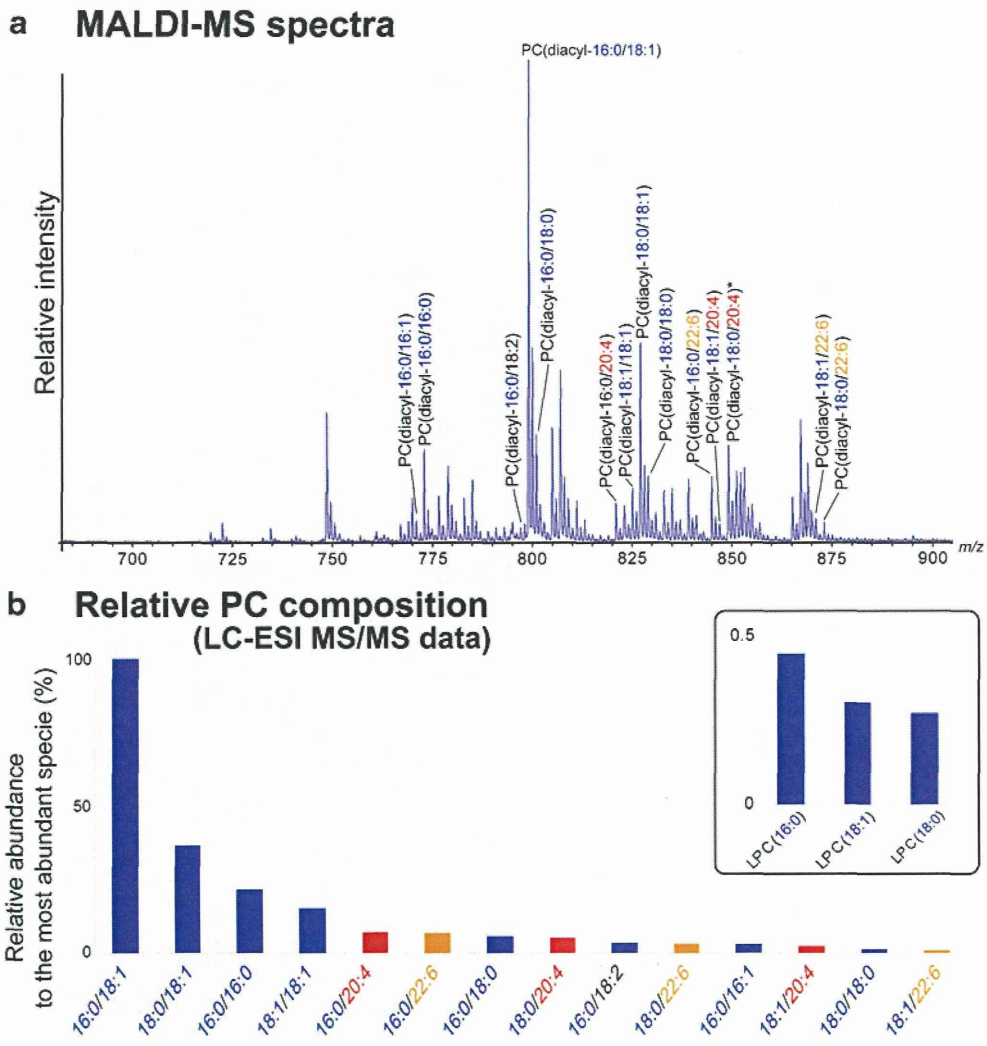

Fig. 1a–b Characterization of primary PC molecular species in normal rat spinal cord. **a** A representative mass spectrum obtained from an entire normal spinal cord section by IMS. In the spectrum, intense mass peaks corresponding to ten abundant PCs were assigned based on their masses and previously reported data. **b** Relative abundances of the 14 principal PC molecular species in the spinal cord block were quantified by monitoring ion transitions from intact PC ions to a fragment ion at *m/z* 184, which is a PC head group. The *y*-axis of the chart represents the percentage abundance of each PC molecular species relative to the most abundant species, PC (diacyl-16:0/18:1)

900 were detected. Among these peaks, 14 intense mass peaks were assigned to abundant PC molecular species based on their masses and previously reported data [12]. Subsequently, LC-ESI-MS/MS was employed in MRM mode to quantify the relative composition of the 14 PC molecular species in the spinal cord block by monitoring ion transitions from intact PC ions to a fragment ion of *m/z* 184, which is a PC head group ion (Fig. 1b). As can be seen from Fig. 1a and 1b, the relative abundance of each PC molecular species is in good agreement with the relative peak/height ratio observed in MALDI-IMS spectra. In addition, trace amounts of lysophosphatidylcholine (LPC) species were detected, and their relative abundances are shown (Fig. 1b, inset).

The tissue distributions of the twelve major PC molecular species in the spinal cord section were subsequently visualized (Fig. 2). The most abundant molecular PC species (diacyl-16:0/18:1) was uniformly distributed across the entire gray matter region of the spinal cord. However, the specific fatty acid compositions of some other species resulted in unique localization features. In particular, with the exception of the (16:0/18:1) species, PCs with oleic acid (18:1), i.e., PC (diacyl-18:0/18:1) and PC(diacyl-18:1/18:1), were frequently localized in the white matter region. Similarly, previous studies have shown that oleic acid-containing PCs are enriched in the myelin sheath structure of the CNS [16, 29, 30]. Moreover, 3-docosahexaenoic acid (DHA)-containing species, i.e., PC (diacyl-16:0/22:6), PC(diacyl-18:0/22:6), and PC(diacyl-18:1/22:6), were frequently localized to gray matter regions. In particular, the close-up distribution of PC(diacyl-16:0/22:6), this PC molecular specie enriched in a region of the large nucleus of motor neurons of the anterior horn, indicated that this DHA-PC was selectively produced by the motor neurons and composed their cellular membrane (Fig. 2a, b; arrowheads).

Irreversible reductions in DHA-containing PCs at one day after SCI

Spatiotemporal changes in PCs were examined by generating relative-abundance maps on the tissue sections at different SCI stages and proximal/distal positions. Analyses were

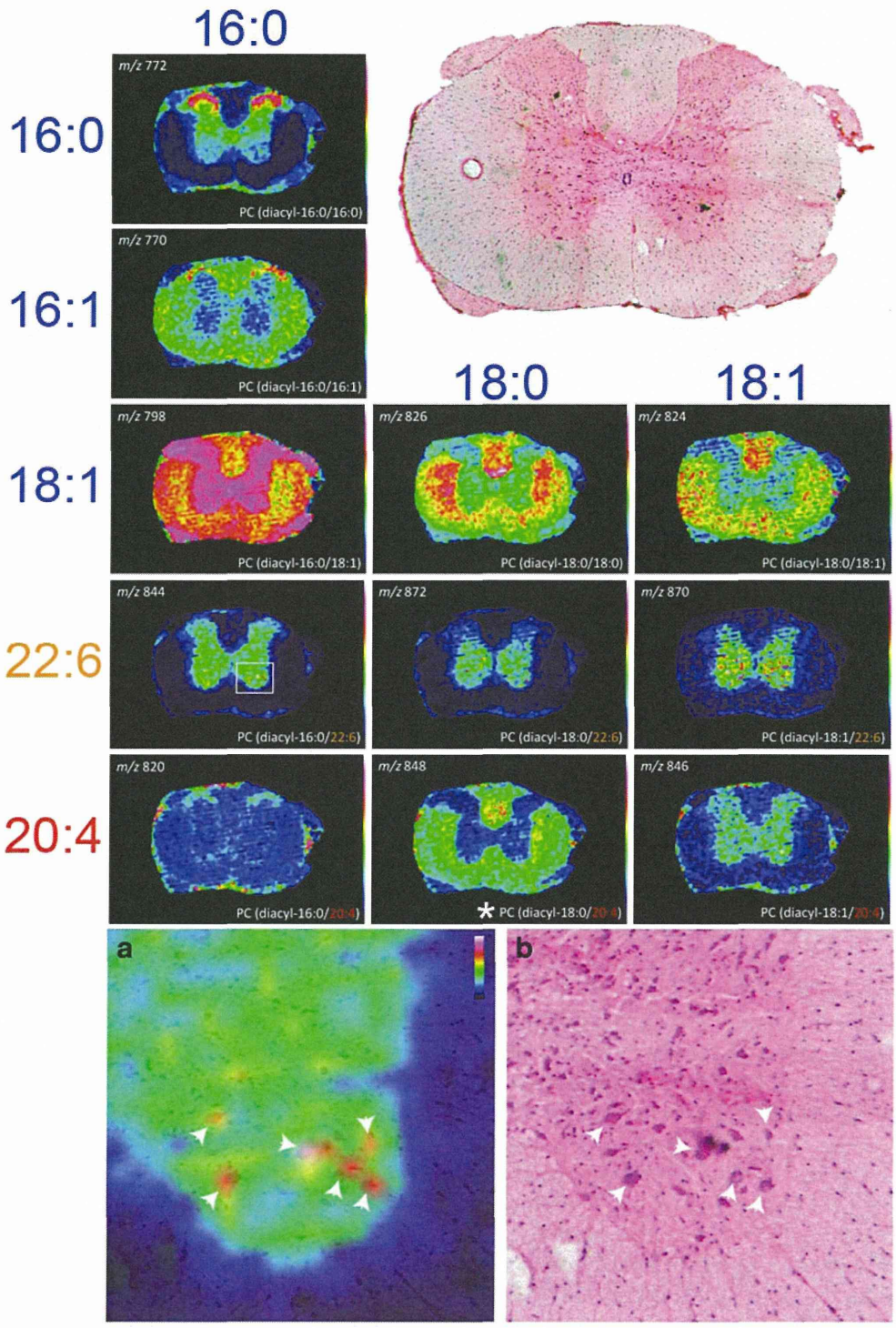

Fig. 2a–b Differential distribution of PC molecular species in a normal spinal cord section. An optical image of H&E-stained rat spinal cord section and ion images of PCs obtained from the same section by IMS are shown. Ion images of PCs are arranged according to their fatty acid (FA) compositions; PCs with identical FA compositions at the *sn*-1 position are arranged lengthwise, while those with identical FA compositions at the *sn*-2 position are arranged horizontally. The specific fatty acid composition is associated with several unique localization features. * Possible contamination of the PC(diacyl-18:0/20:4) signal at *m/z* 848 with sodiated species of galactosylceramide (d18:1/h24:1). **a**, **b** Detailed distribution of PC(diacyl-16:0/22:6), a PC molecular species enriched in a region of the large nucleus in the anterior horn. The *arrowheads* indicates anterior horn cells

performed on 24 sections from sham-operated and injured groups during a period of 12 h to 8 weeks post-SCI (n=3 for each group). A total of four different cross-sections located from the proximal to the distal side, including the impact site, were assessed. As a result, we found both temporal and irreversible alterations in distinct PC molecular species, particularly for those containing polyunsaturated fatty acids (PUFAs), i.e., arachidonic acid (AA)- and DHA-containing PCs. Furthermore, PCs containing the same PUFA showed similar alteration patterns. We additionally note that the IMS results from sham-operated samples, which had been laminectomized, indicated no significant alteration in PC content except for LPC(16:0) (see Fig. S2 of the ESM).

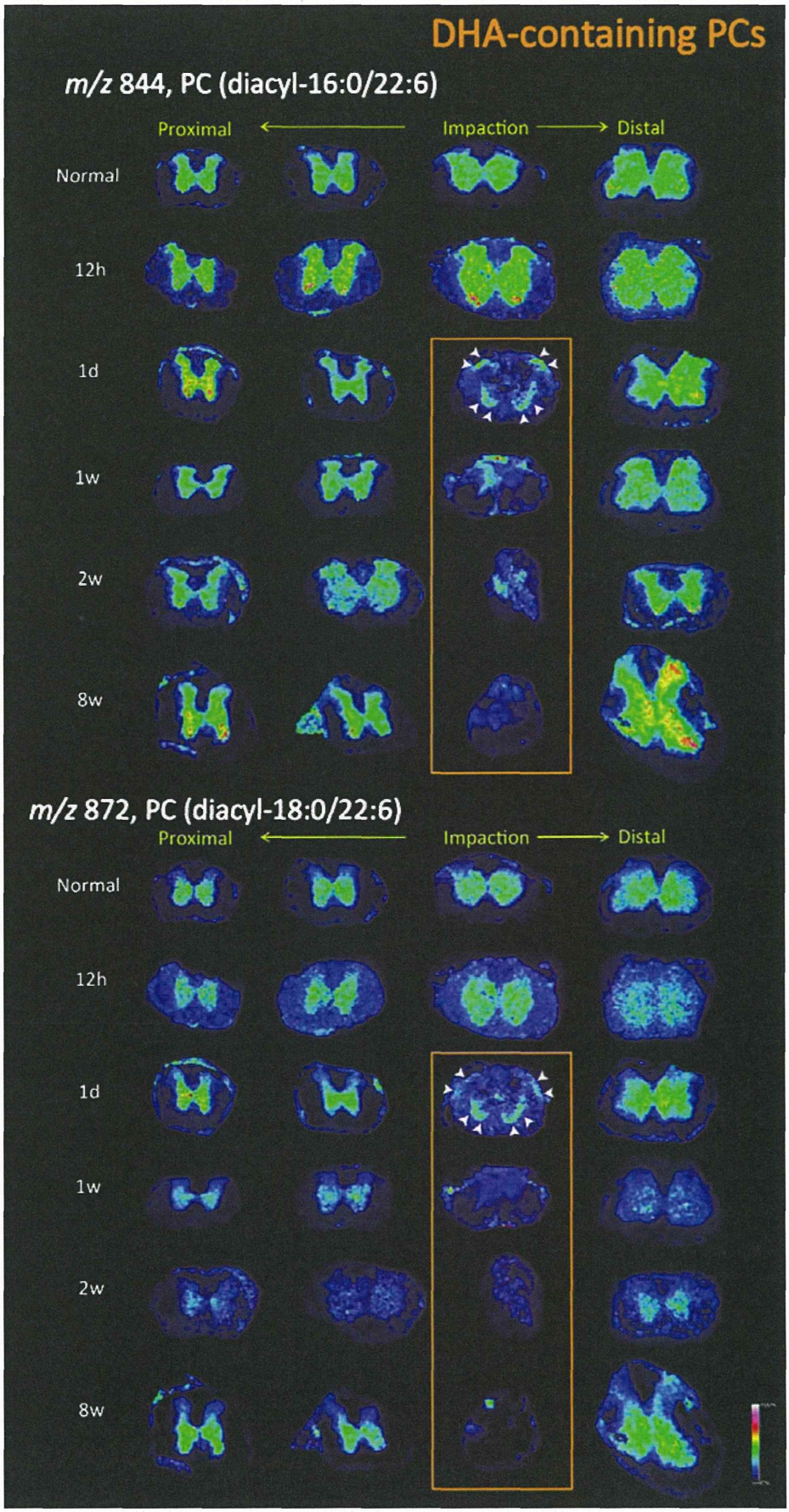

Fig. 3 DHA-containing PCs exhibited impact site-specific irreversible reductions from 1 day to 8 weeks post-SCI. The IMS results for DHA-containing PCs, i.e., PC(diacyl-16:0/22:6) and PC (diacyl-18:0/22:6), are detailed. In particular, the 24 ion images for each DHA-PC from sections of normal (sham-operated) and SCI-treated samples at five different time points are shown. The distribution of DHA-PCs was unaltered at 12 h post-SCI in comparison with the control. The primary reduction was observed around the central canal and gray commissure region to a severe extent at 1 d post-SCI, whereas the decreases at the anterior and posterior horns were moderate (*arrowheads*). However, at 1 week post-SCI, DHA-PCs were also lost from these tissue regions, and these reductions evolved at later time points and the DHA-PCs had almost disappeared by 8 weeks post-SCI

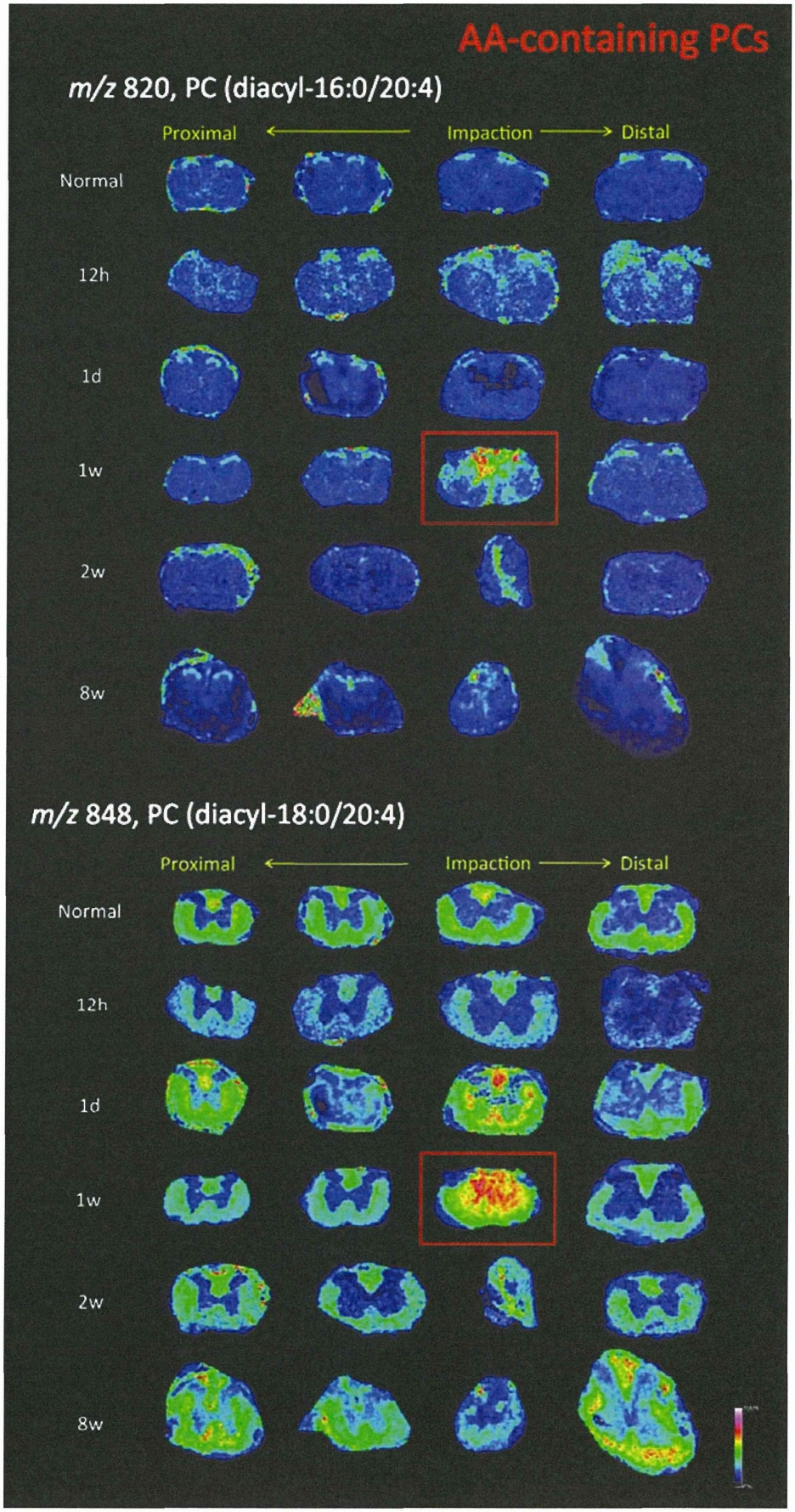

Fig. 4 Temporary elevations in AA-containing PCs after SCI. The IMS results for the AA-containing PCs, i.e., PC (diacyl-16:0/20:4) and PC (diacyl-18:0/20:4), are detailed. In particular, 24 ion images for each AA-PC from sections of normal (sham-operated) and SCI-treated samples at five different time points are shown. As shown in the *red square*, both AA-PCs showed intense increases at the impact site by 1 week post-SCI, while lower or almost no alterations were found at other tissue locations. The elevations were observed as temporary events and had resolved by 8 weeks post-SCI